

Supplementary information

Fluorogenic probes for live-cell imaging of the cytoskeleton

Gražvydas Lukinavičius^{1,8}, Luc Reymond^{1,2,8}, Elisa D'Este³, Anastasiya Masharina¹, Fabian Göttfert³, Haisen Ta³, Angelika Güther⁴, Mathias Fournier⁵, Stefano Rizzo⁶, Herbert Waldmann⁶, Claudia Blaukopf⁷, Christoph Sommer⁷, Daniel Wolfram Gerlich⁷, Hans-Dieter Arndt⁴, Stefan W Hell³, and Kai Johnsson^{1,2}

¹ Institute of Chemical Sciences and Engineering, École Polytechnique Fédérale de Lausanne, Lausanne, Switzerland

² National Centre of Competence of Research in Chemical Biology, Switzerland

³ Department of NanoBiophotonics, Max-Planck-Institute for Biophysical Chemistry, Göttingen, Germany

⁴ Institute of Organic Chemistry and Makromolecular Chemistry, Friedrich-Schiller-University, Jena, Germany

⁵ Bioimaging and Optics platform, École Polytechnique Fédérale de Lausanne, Lausanne, Switzerland

⁶ Max-Planck-Institute of Molecular Physiology, Dortmund, Germany

⁷ Institute of Molecular Biotechnology of the Austrian Academy of Sciences, Vienna, Austria

⁸ These authors contributed equally to this work

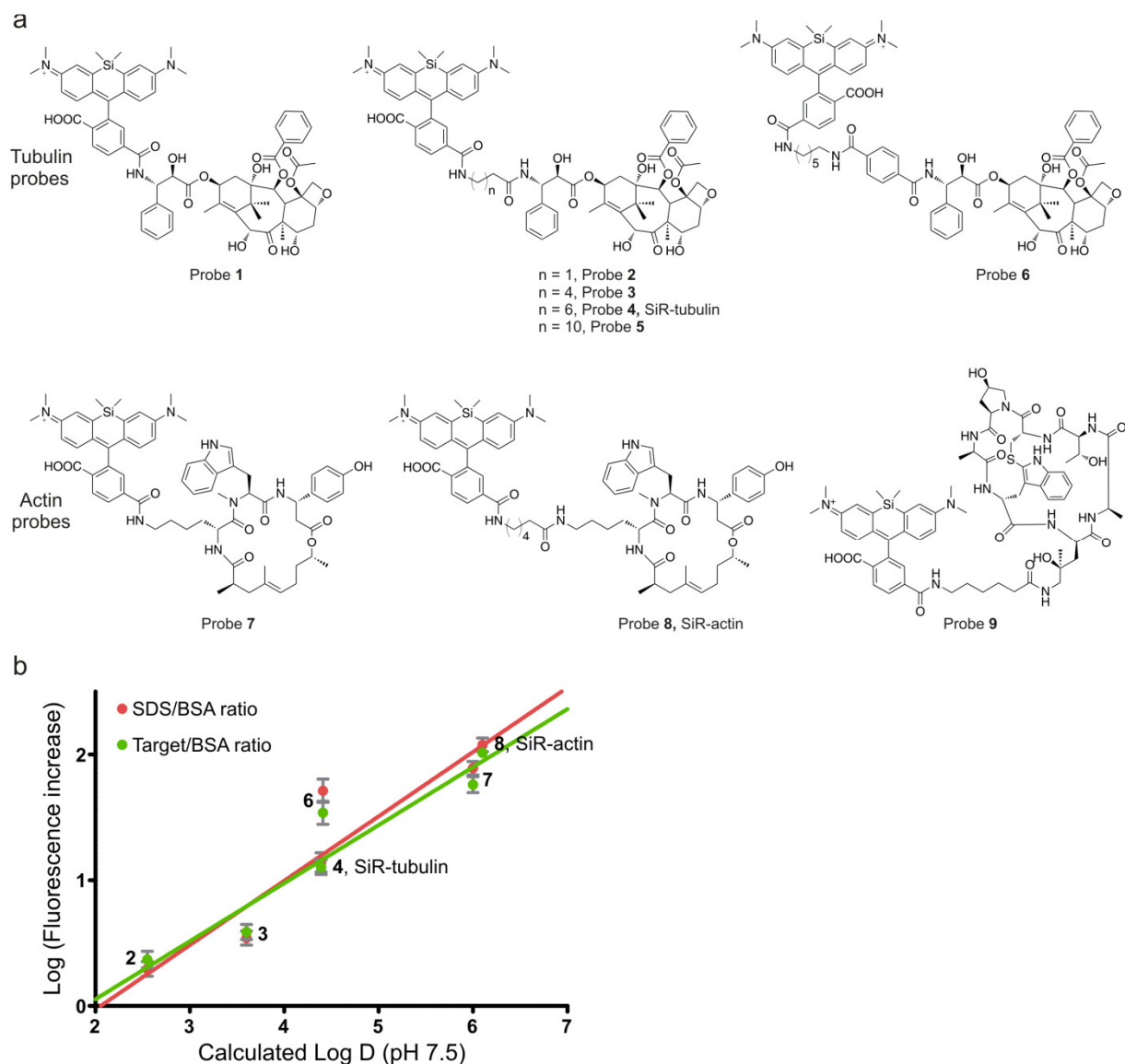
Corresponding authors e-mails: kai.johnsson@epfl.ch, hd.arndt@uni-jena.de, shell@gwdg.de .

Supplementary inventory

Supplementary Figures	3
Supplementary Figure 1. SiR-tubulin and SiR-actin probes.	3
Supplementary Figure 2. Spectral properties of actin and tubulin probes.	4
Supplementary Figure 3. Visualization of microtubule and actin cytoskeleton by SiR-probes in live cells at different cell cycle stages using confocal microscopy.	5
Supplementary Figure 4. Staining of human primary dermal fibroblasts expressing GFP-tubulin with tubulin probes.	6
Supplementary Figure 5. Staining of human primary dermal fibroblasts expressing RFP-actin with actin probes.	7
Supplementary Figure 6. Imaging of actin in intact red blood cells (RBC).	8
Supplementary Figure 7. Effect of SiR probes on actin and tubulin polymerization / depolymerization in vitro.	10
Supplementary Figure 8. Testing cytotoxicity of SiR-tubulin (top) and SiR-actin (bottom).	12
Supplementary Figure 9. Long-term live-cell microscopy of HeLa Kyoto cells stained with SiR-probes.	13
Supplementary Figure 10. SIM and STED microscopy of living cells stained with the SiR-tubulin probe.	15
Supplementary Figure 11. Measurement of the polar angle in-between neighboring intensity maxima of the centriole stained with SiR-tubulin.	17
Supplementary Figure 12. Images of SiR-actin-stained living primary rat hippocampal neurons at 16 days in vitro.	19
Supplementary Figure 13. Lifeact fails in detecting actin rings in living primary rat hippocampal neurons.	20
Supplementary Figure 14. Comparative staining of PFA fixed human primary dermal fibroblasts with actin probes.	21
Supplementary Tables.	22
Supplementary Table 1. Staining different cell lines with SiR-actin and SiR-tubulin probes.	22
Supplementary Table 2. Properties of the synthesized probes.	22
Supplementary Table 3. Physicochemical properties of the synthesized probes.	23
Supplementary notes.	24
Supplementary Note 1. Design and properties of the SiR-tubulin probe.	24
Supplementary Note 2. Chemical synthesis of tubulin and actin probes.	25
Supplementary Note 3. Toxicity of the SiR-tubulin and SiR-actin probes.	35
Supplementary references	36

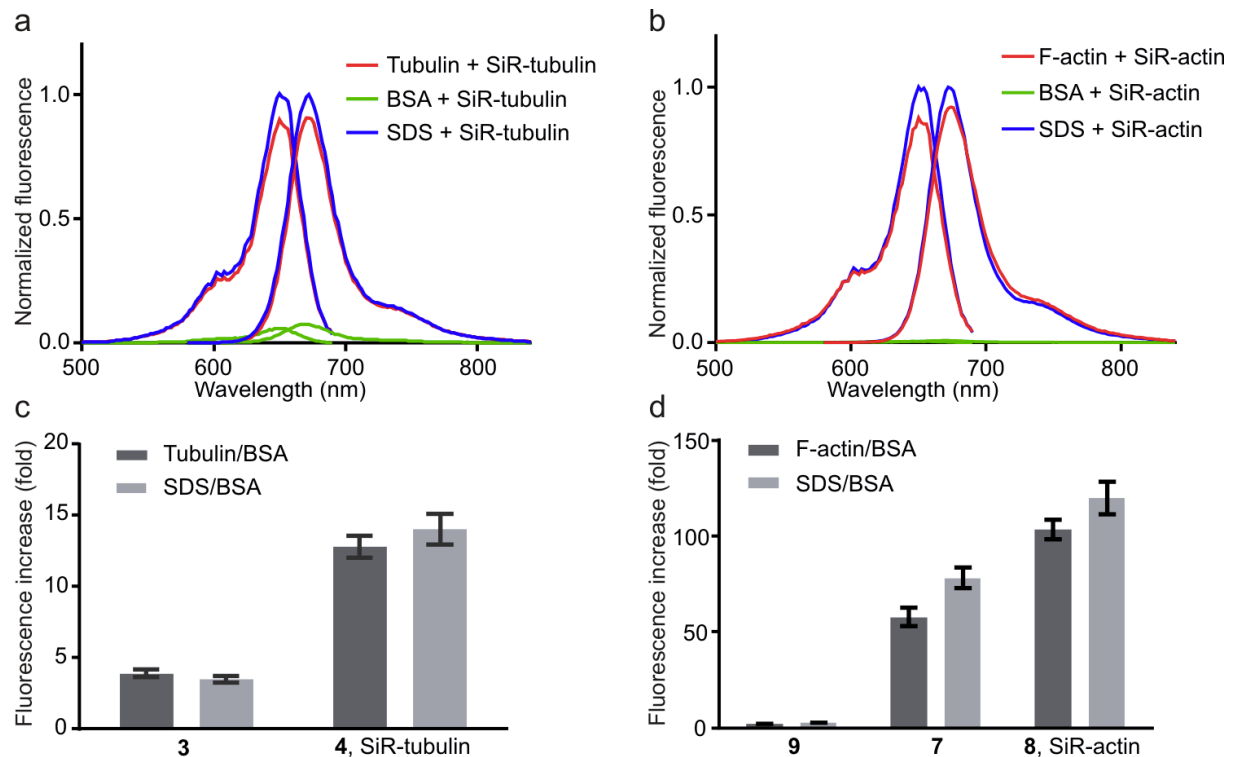
Supplementary Figures

Supplementary Figure 1. SiR-tubulin and SiR-actin probes.



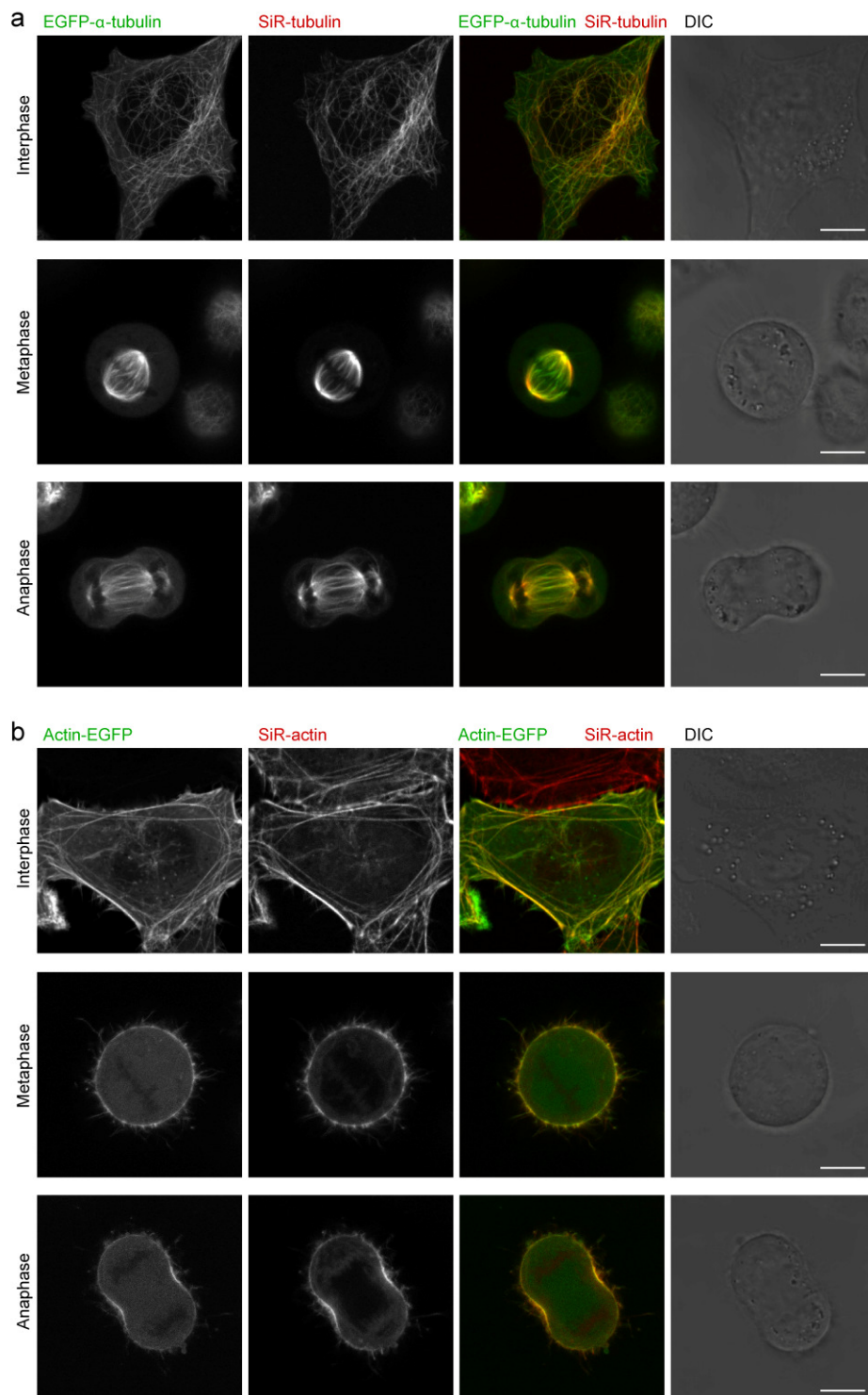
(a) Chemical structures of synthesized tubulin and actin probes. For chemical synthesis details please see **Supplementary Note 2**. (b) Fluorescence increase at 672 nm upon target binding or 0.2% SDS addition of SiR-based tubulin and actin probes correlates well with calculated Log D value. Each dot represents the mean value with standard error of the mean (SEM) as error bars ($n \geq 3$).

Supplementary Figure 2. Spectral properties of actin and tubulin probes.



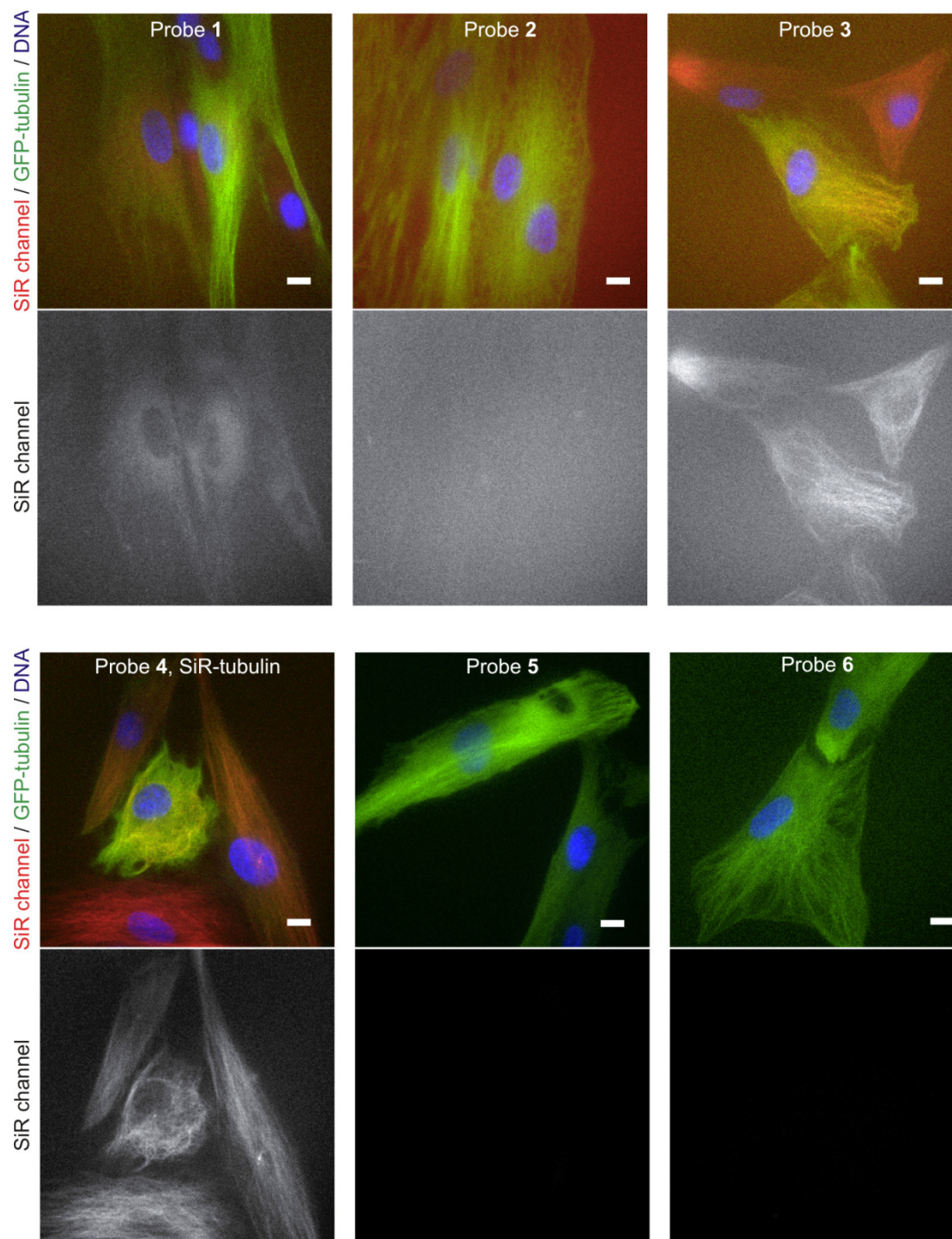
(a) Fluorescence excitation and emission spectra of SiR-tubulin bound to polymerized tubulin, in presence of BSA or 0.2% SDS. All spectra were normalized to values of the fluorescence spectra recorded in presence of SDS. **(b)** Fluorescence excitation and emission spectra of SiR-actin bound to polymerized F-actin, in presence of BSA or 0.2% SDS. All spectra were normalized to values of the fluorescence spectra recorded in presence of 0.2% SDS. **(c)** Comparison of fluorescence intensity increase at 672 nm of the tubulin probes upon addition of SDS or binding to tubulin. **(d)** Comparison of fluorescence intensity increase at 672 nm of the actin probes upon addition of SDS or binding to F-actin. Each column represents the mean value with standard error of the mean (SEM) as error bars ($n \geq 3$).

Supplementary Figure 3. Visualization of microtubule and actin cytoskeleton by SiR-probes in live cells at different cell cycle stages using confocal microscopy.



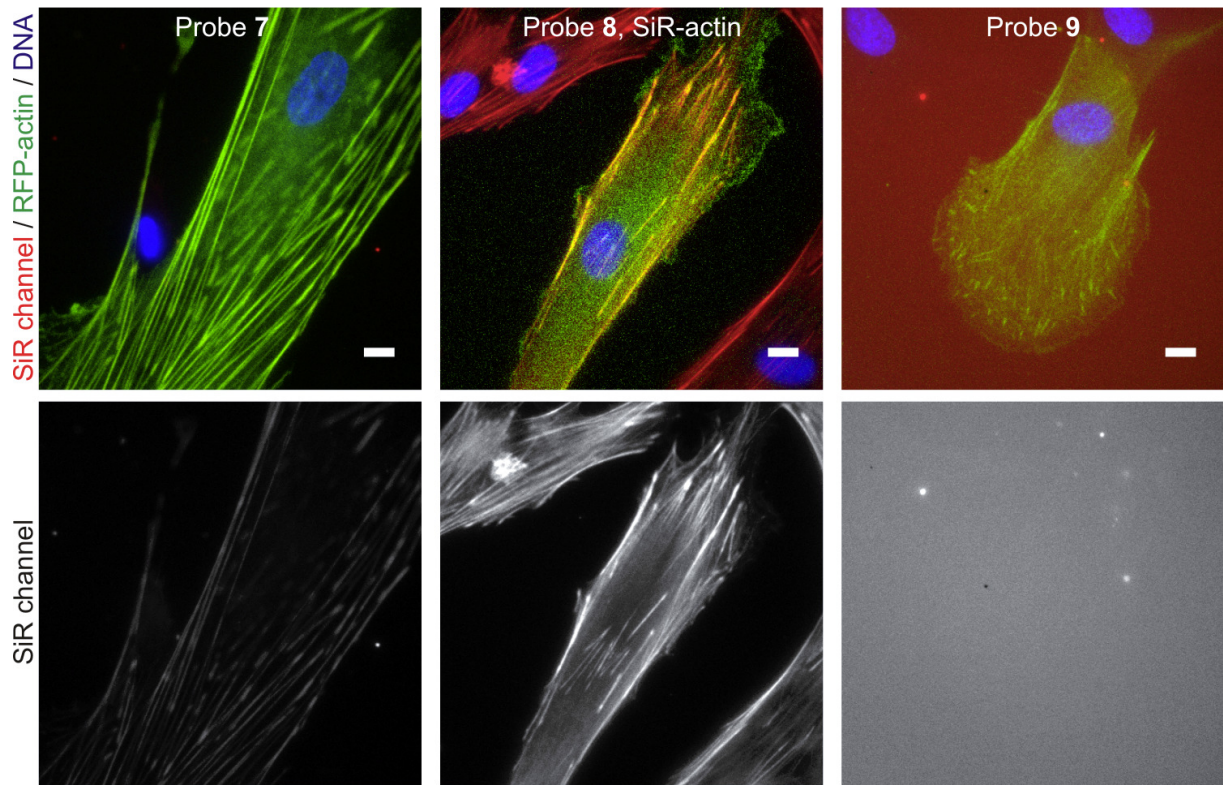
(a) 100 nM SiR-tubulin was added to the culture medium 20 h prior to live-imaging of HeLa Kyoto cells stably expressing mEGFP- α -tubulin ($n = 23$ cells). **(b)** 100 nM SiR-actin was added to the culture medium 20 h prior to live-imaging HeLa Kyoto cells stably expressing actin-EGFP ($n = 26$ cells). Scale bars - 10 μ m.

Supplementary Figure 4. Staining of human primary dermal fibroblasts expressing GFP-tubulin with tubulin probes.



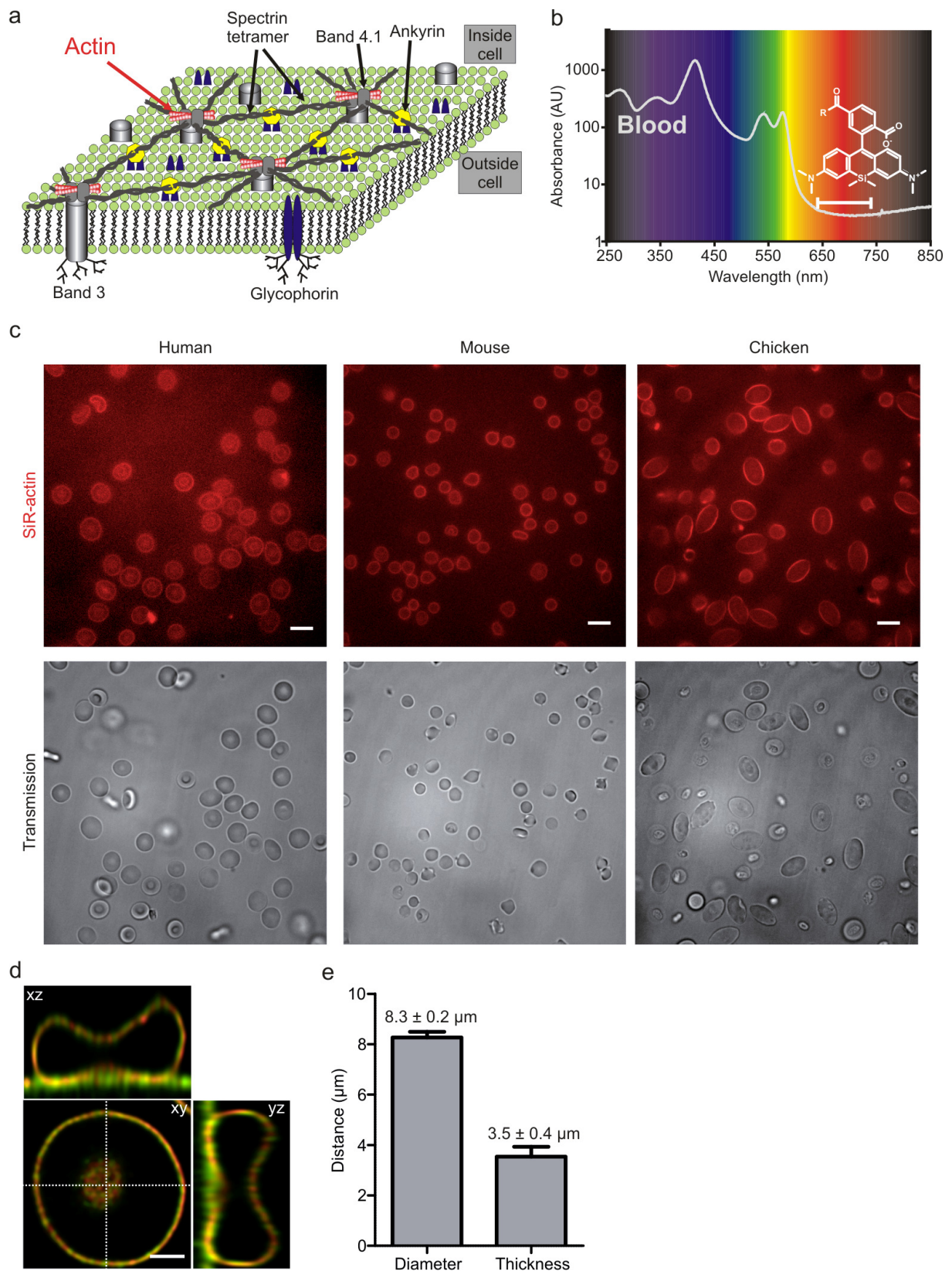
Living cells were incubated with 1 μ M probe in presence of 1 μ g / ml Hoechst 33342 for 60 min and imaged on a Leica DMI6000B wide field microscope without washing off excess of probe. Images represent a single focal plane. Scale bars - 10 μ m.

Supplementary Figure 5. Staining of human primary dermal fibroblasts expressing RFP-actin with actin probes.



Living cells were incubated with 1 μ M probe in presence of 1 μ g / ml Hoechst 33342 for 60 min and imaged on a Leica DMI6000B wide field microscope without washing off excess of probe. Images represent a single focal plane. Scale bars - 10 μ m.

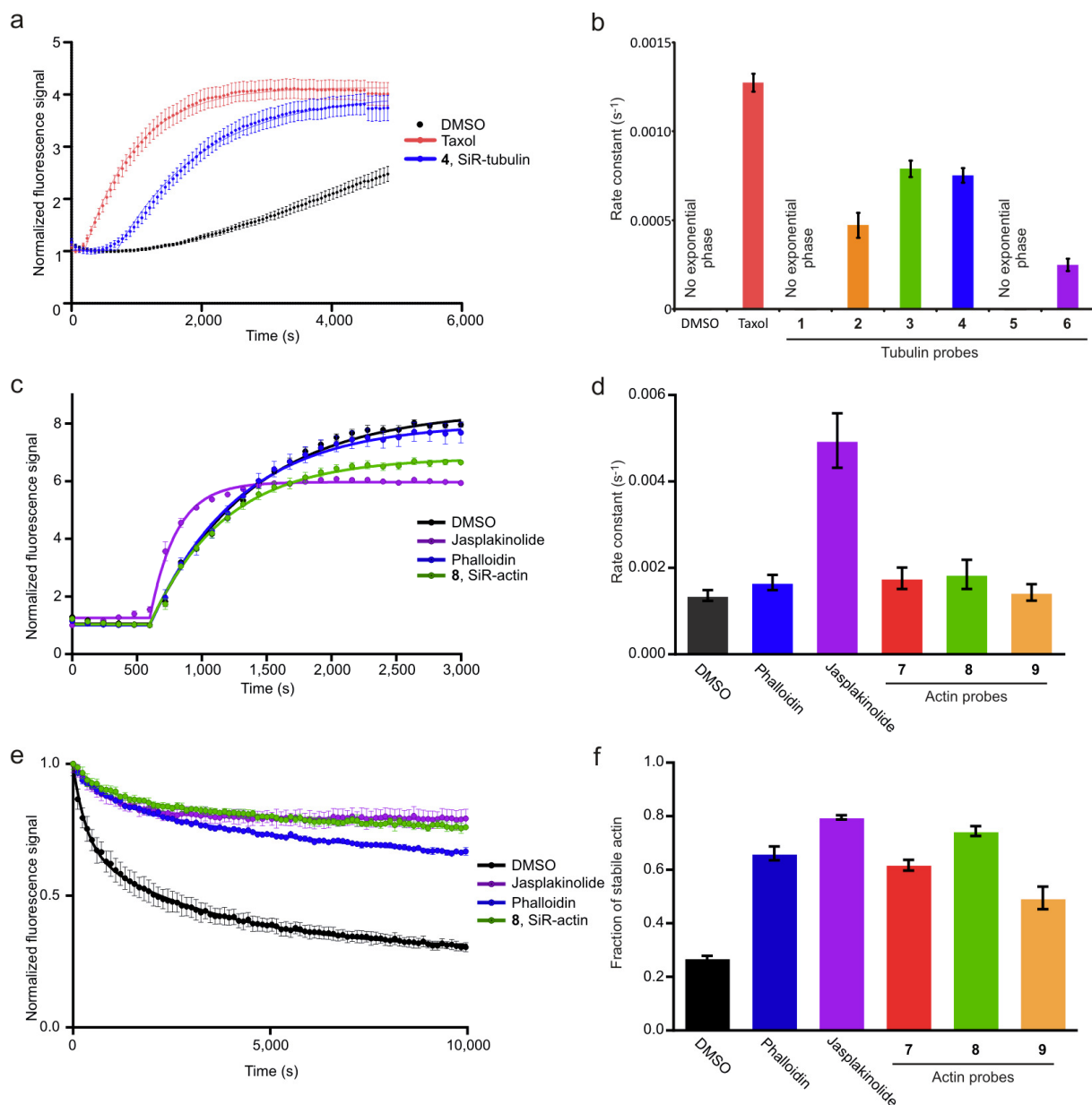
Supplementary Figure 6. Imaging of actin in intact red blood cells (RBC).



(a) Model showing the composition of a human erythrocyte membrane skeleton. **(b)** SiR-based probes are excited and emit light in the far-red spectral range which is

outside the maximal absorbance of blood. The spectrum shows absorbance of mouse whole blood that was osmotically lysed. (c) Images of erythrocytes stained with 5 μM SiR-actin probe for 30 min and imaged on a Leica DMI6000B microscope without washing off the probe. Images represent a single focal plane. Scale bar - 10 μm (d) 3D reconstruction of the human erythrocyte imaged with a confocal Leica SP5 microscope. The membrane of the erythrocyte was stained with BODIPY® FL-C5-ceramide (green) and actin was stained with the SiR-actin probe (red). Dotted lines indicate xz and yz cross-sections. Scale bar - 2 μm . (e) Measured diameter and thickness of human RBC is in good agreement with values reported in literature (diameter 6 – 8 μm , thickness 2 - 3 μm)¹. Each column represents the mean value with standard deviation as error bars. Number of measured RBC = 10.

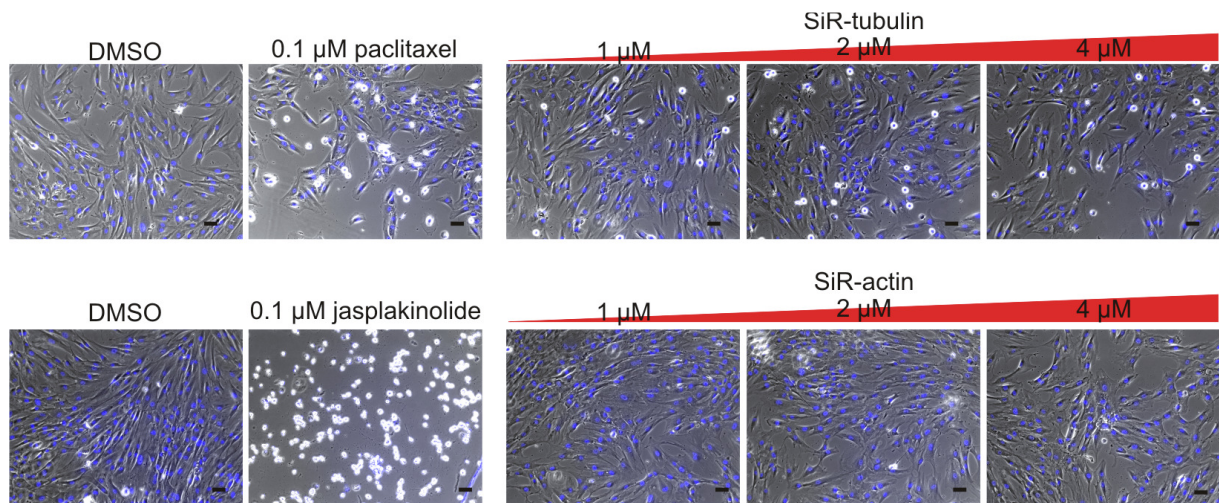
Supplementary Figure 7. Effect of SiR probes on actin and tubulin polymerization / depolymerization in vitro.



(a) Representative experiment of a tubulin polymerization assay. Obtained fluorescence increase was fitted to an equation describing "plateau followed by exponential increase" (see methods part for details). (b) Summary of obtained rate constant values of the exponential growth phase of tubulin polymerization. (c) Representative experiment of a pyrene labeled actin polymerization assay. Obtained fluorescence increase was fitted to an equation describing "plateau followed by exponential increase" (see methods part for details). (d) Summary of obtained rate constant values of the exponential growth phase of pyrene labeled actin polymerization. (e) Representative experiment of pyrene actin depolymerization

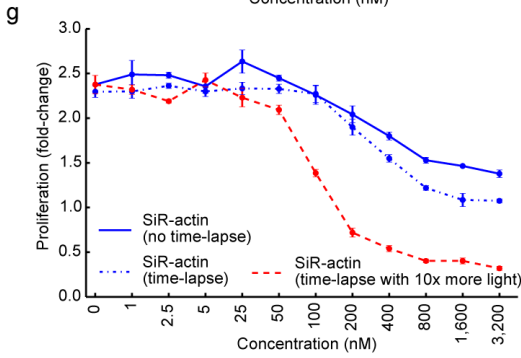
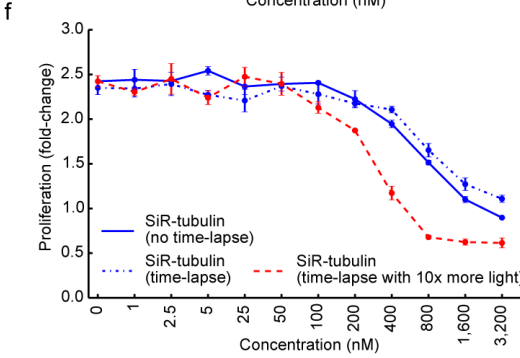
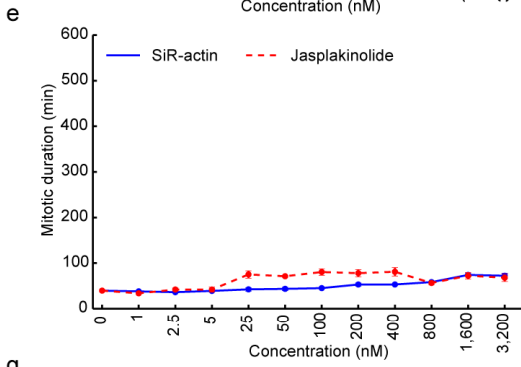
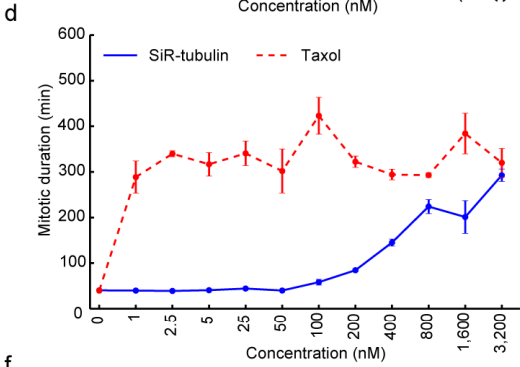
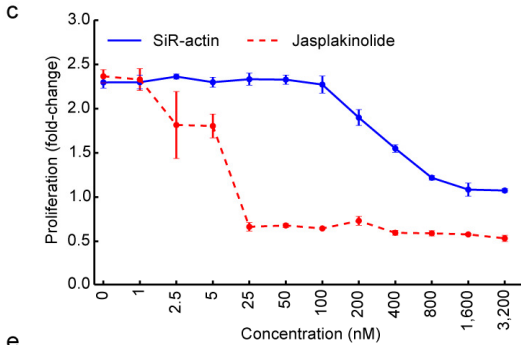
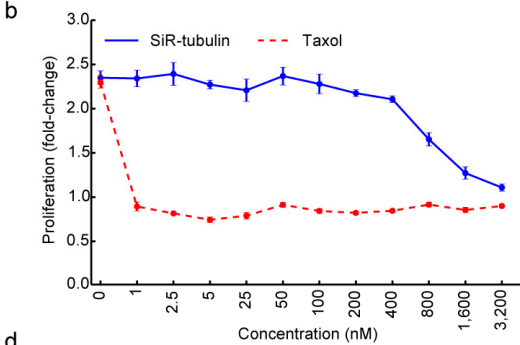
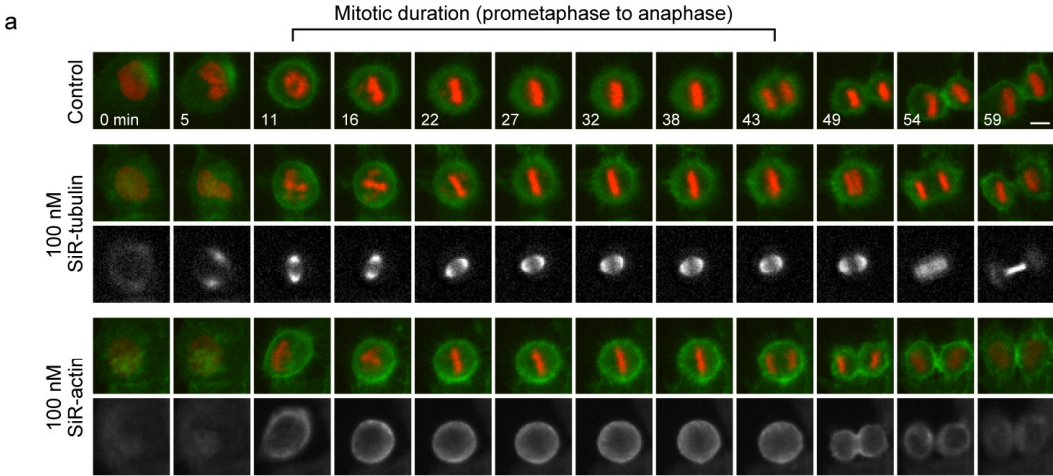
assay. Obtained fluorescence decrease was fitted to a bi-exponential decay equation (see methods part for details). The fitted plateau value is proportional to the fraction of stabilized actin. **(f)** Summary of the obtained plateau values for stable actin. Each column represents the mean of two or more independent experiments with standard error of the mean (SEM) as error bars. Graphs of representative experiments show means of technical duplicates or triplicates with SEM as error bars.

Supplementary Figure 8. Testing cytotoxicity of SiR-tubulin (top) and SiR-actin (bottom).



Human primary dermal fibroblasts were grown in media containing the indicated concentrations of probes or control compounds for 24 h at 37 °C in humidified atmosphere containing 5% CO₂. Cells were stained with 1 μg / ml Hoechst 33342 for 60 min and imaged on a Zeiss Axiovert 200 system. Images represent the overlay of single focal planes of Hoechst 33342 (blue) fluorescence and phase contrast (gray). Note that bright dots in the images are rounded cells which cannot accomplish mitosis or cannot grow on flat surface due to cytoskeleton modifications. Scale bars - 50 μm.

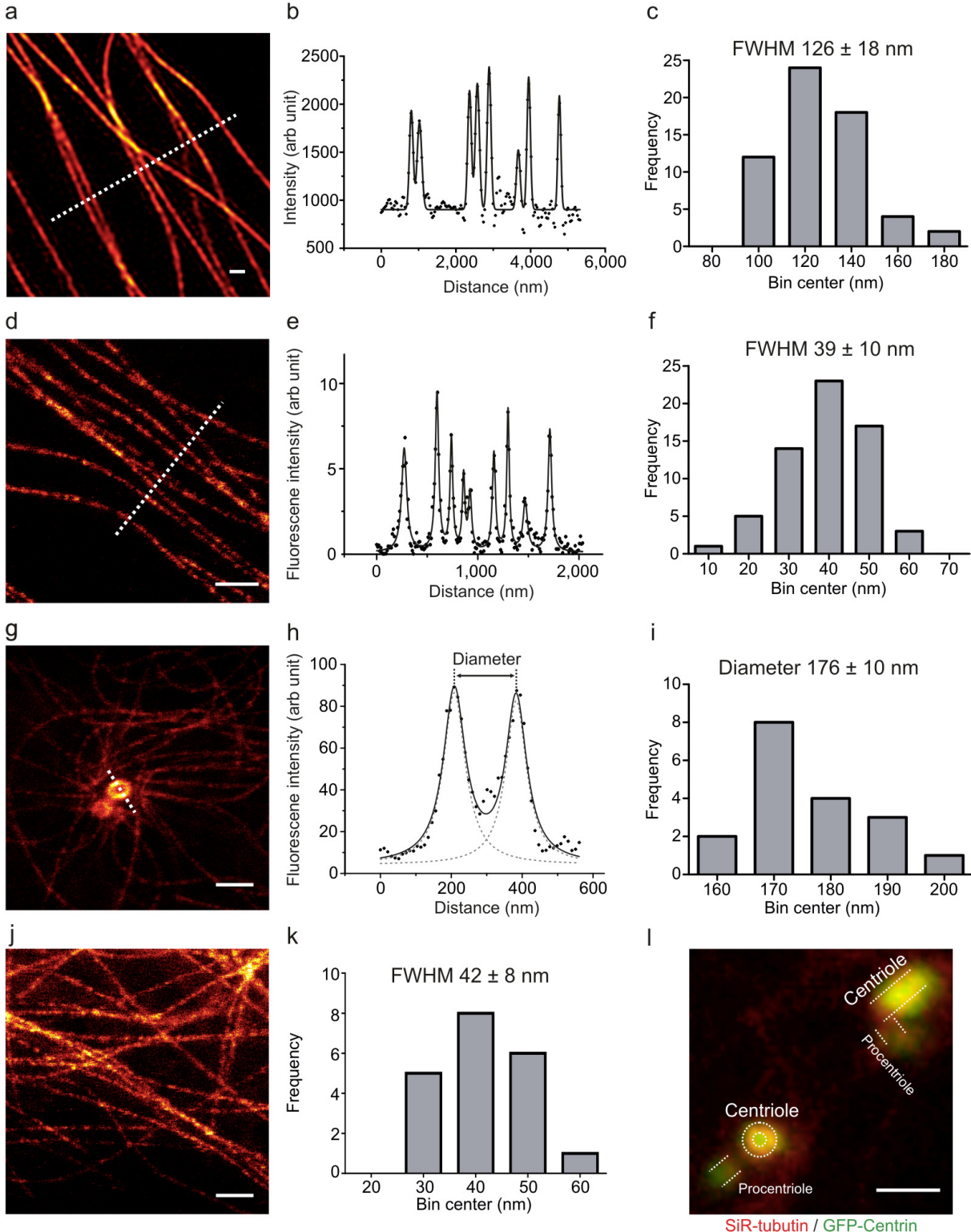
Supplementary Figure 9. Long-term live-cell microscopy of HeLa Kyoto cells stained with SiR-probes.



SiR-tubulin or SiR-actin was added to HeLa cells expressing H2B-mRFP and MyrPalm-mEGFP, at different concentrations between 1 nM and 3.2 μM. Time-lapse

recordings were started 30 min after probe addition (no washing of the probe) on a wide-field epifluorescence microscope. Time-lapse images were taken each 5.4 min, total movie duration was 23 h. **(a)** Representative dividing cells from movies of untreated controls, or cells treated with 100 nM SiR-tubulin or SiR-actin, respectively. More cells are shown in **Supplementary Video 1-3**. Scale bar - 10 μm . **(b, c)** Quantification of cell proliferation in cells imaged as described above. Cells were treated with different concentrations of the SiR-probes, taxol, or jasplakinolide. Proliferation was measured by automated segmentation and classification of live and dead cells. Proliferation is calculated as the ratio of all live cells in the last frame of the movie (23 h) divided by all live cells detected in the first frame. All compounds were present in media throughout the entire imaging duration. **(d, e)** Quantification of mitotic duration in the imaging data shown in **(a-c)**. Interphase, 4 mitotic stages, and apoptosis were classified by supervised machine learning in trajectories of dividing cells. Mitotic duration was measured from prometaphase until anaphase, as illustrated in **(a)**. Please note that only very few cells entered mitosis in the presence of jasplakinolide, and only during the first two hours of the movie, owing to the high toxicity of this drug (**Supplementary Video 5**). **(f, g)** Quantification of cell proliferation at different light exposures and drug concentrations to assay for photo-toxicity dependence on SiR-probes. Cells were prepared and treated as in **(b)** and **(c)** but then imaged in a single frame 30 min after drug addition, and 23 h (no time-lapse), or at a time-lapse similar to **(b)** and **(c)**, but with 10-fold higher illumination intensity in the SiR-probe imaging channel. Quantification of cell proliferation from **(b)** and **(c)** is also shown in **(f)** and **(g)**, respectively. The data shown **(b-g)** are mean \pm SEM (n = 3).

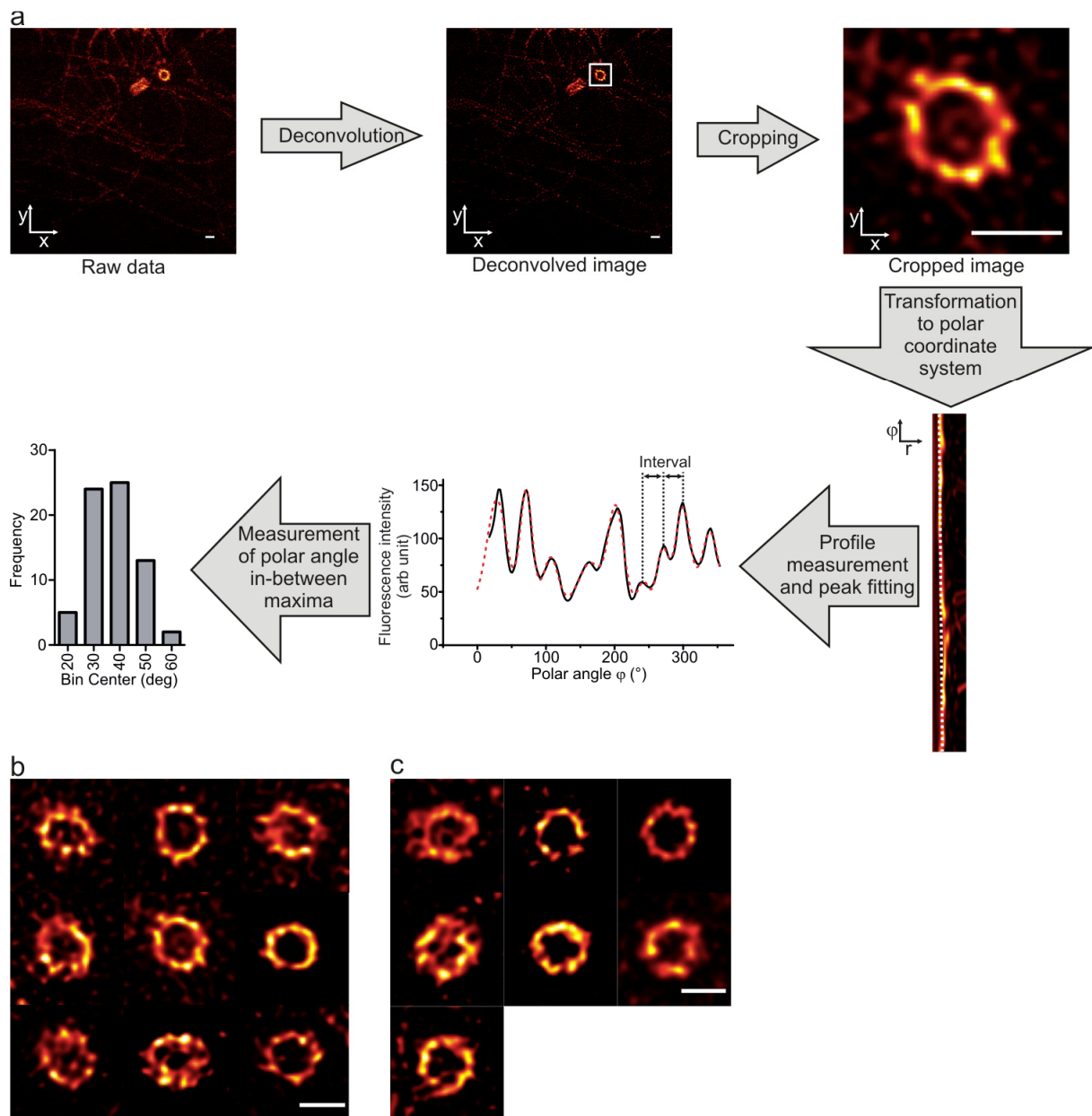
Supplementary Figure 10. SIM and STED microscopy of living cells stained with the SiR-tubulin probe.



(a) 3D SIM microscopy image of microtubules labeled with SiR-tubulin in human primary dermal fibroblasts. (b) Intensity line profile along the white dotted line marked in (a). (c) Histogram of the measured full width at half maximum (FWHM) of the

microtubules. The FWHM of the imaged structures was obtained by fitting fluorescence intensity profiles to multiple Gaussian distributions (OriginPro 9, <http://www.originlab.com/>). 3D SIM image was obtained on Nikon Eclipse Ti microscope. **(d)** STED microscopy image of the microtubules labeled with SiR-tubulin in human primary dermal fibroblasts. **(e)** Intensity line profile along the white dotted line marked in **(d)**. **(f)** Histogram of the measured FWHM of the microtubules. **(g)** STED microscopy image of a centrosome stained with SiR-tubulin in human primary dermal fibroblasts. Diffuse signal visible near the doughnut shaped centriole signal is the second centriole which is located outside the focal plane. **(h)** Intensity line profile along the white dotted line marked in **(g)**. Two separated Lorentz distributions are indicated by grey dashed lines in case of the STED profile fitting. Distance between the peaks of double Lorentz fitting (solid line) was taken as diameter of the structure. **(i)** Histogram shows distributions of the diameter of the centriole. **(j)** STED microscopy image of the microtubules labeled overnight with 100 nM SiR-tubulin in HeLa cells. **(k)** Histogram of the measured FWHM of the microtubules labeled overnight with 100 nM SiR-tubulin in HeLa cells. **(l)** STED microscopy image of the centrosome region stained with SiR-tubulin in HeLa cells expressing GFP-Centrin. GFP-Centrin signal is taken in confocal mode and localizes to the distal end of the centriole and the procentriole. All scale bars - 0.5 μm .

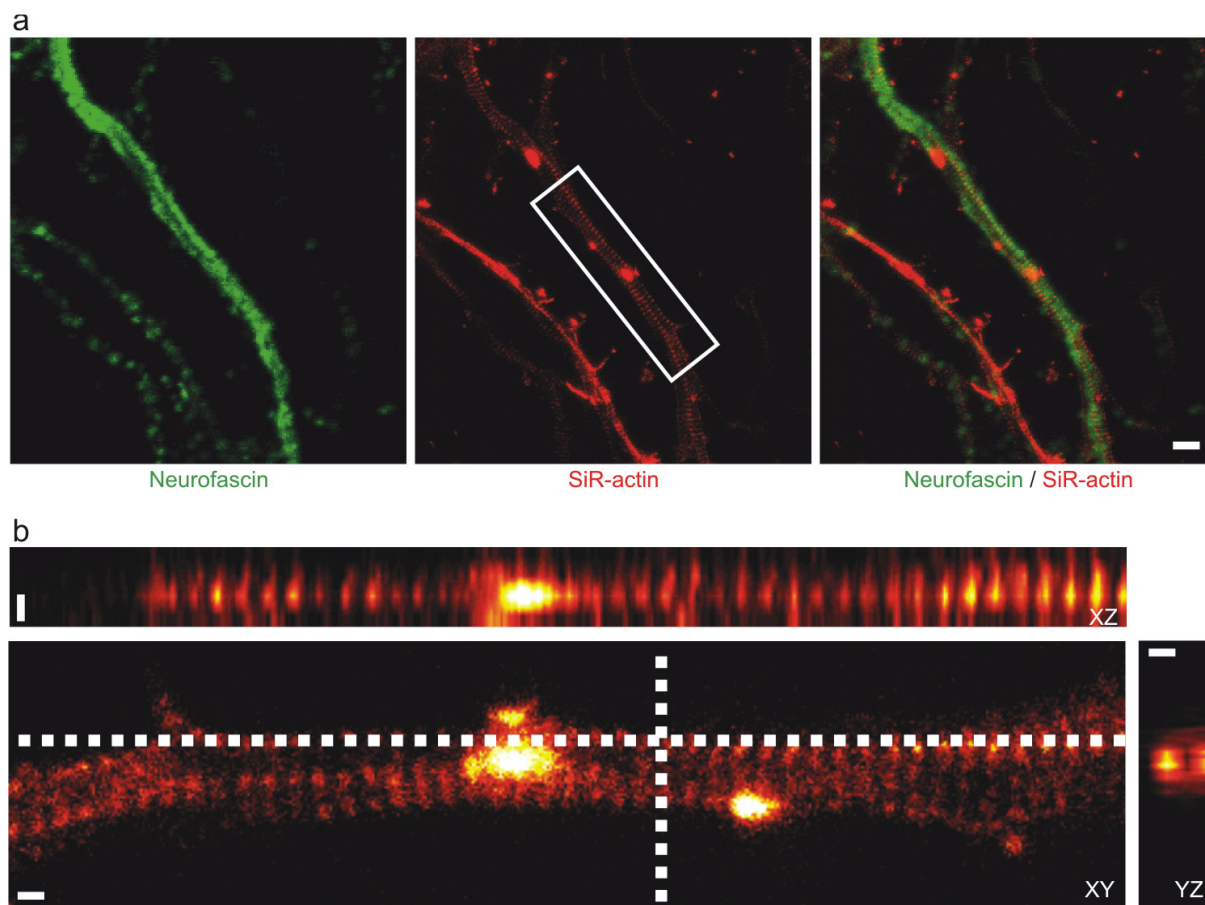
Supplementary Figure 11. Measurement of the polar angle in-between neighboring intensity maxima of the centriole stained with SiR-tubulin.



(a) Example showing the angle measurement of a centriole in living mouse IA32 cells. Raw data were deconvolved using the measured 2D-PSF and cropped. Deconvolution was performed using the Richardson-Lucy algorithm and ImSpector (Max-Planck Innovation) software. The Images have been transformed using a polar transformer plug-in (<http://rsbweb.nih.gov/ij/plugins/polar-transformer.html>) on Fiji ² after cropping so that the center of the centriole ring is close to the center of the image. Intensity profile has been measured (black line), fitted to multiple Gaussian distributions (red dotted line) and intervals between two neighboring fitted peaks were measured using OriginPro 9 (<http://www.originlab.com/>). **(b)** A set of images used to

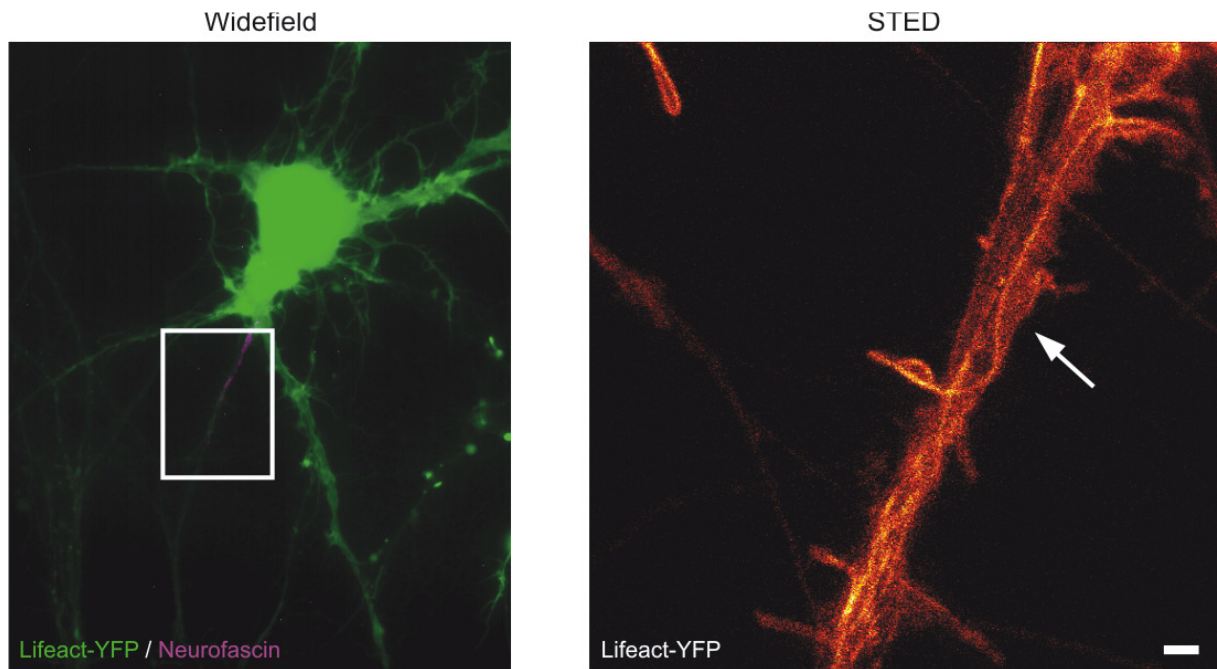
measure the polar angles in-between neighboring intensity maxima of the centriole in mouse IA32 cells. (c) A set of images used to measure the polar angles in-between neighboring intensity maxima of the centriole in human primary dermal fibroblasts. Scale bars - 200 nm.

Supplementary Figure 12. Images of SiR-actin-stained living primary rat hippocampal neurons at 16 days in vitro.



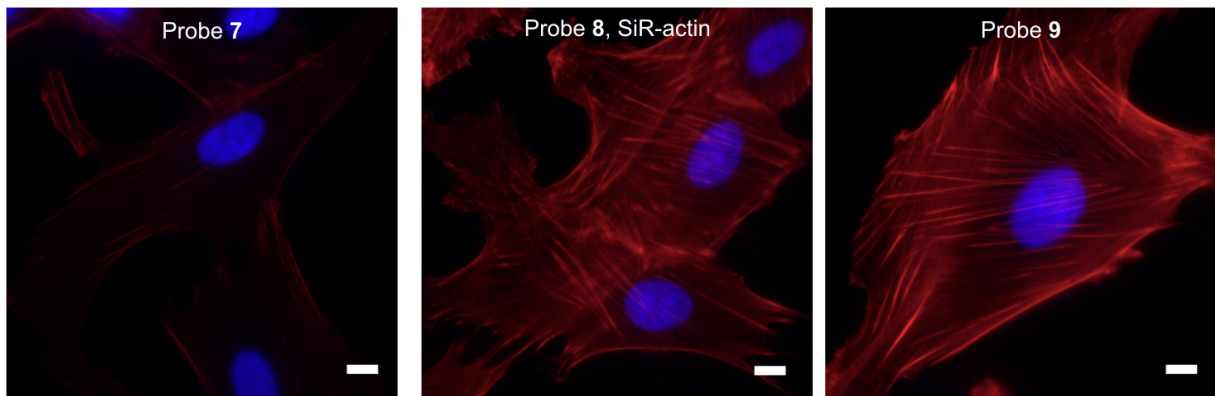
(a) Colocalization of SiR-actin probe signal (red) with antibody labeled axon marker neurofascin (green). SiR-actin is visualized via STED while neurofascin is imaged via confocal microscopy (Supplementary methods). Scale bar - 0.5 μm . **(b)** Orthogonal projections of the z-stack STED image shown in the white rectangle of panel **(a)**. Z-stack was acquired on an in-house build STED microscope. Dotted lines indicate xz and yz plane. Scale bar - 200 nm.

Supplementary Figure 13. Lifeact fails in detecting actin rings in living primary rat hippocampal neurons.



Widefield image of a cell expressing Lifeact-YFP fusion protein (green) and antibody-stained with the axonal marker neurofascin (magenta). The white box indicates the area shown in the STED image on the left (raw data). We speculate that the reason why Lifeact fails in detecting actin rings in these experiments is its higher affinity for G-actin than F-actin³. Arrow indicate the axon. Image was acquired on an in-house build STED microscope. Scale bar – 1 μm .

Supplementary Figure 14. Comparative staining of PFA fixed human primary dermal fibroblasts with actin probes.



PFA fixed cells were incubated with 2 μ M probe (red) in presence of 1 μ g / ml Hoechst 33342 (blue) for 60 min, washed and imaged on a Leica DMI6000B wide field microscope. Images represent a single focal plane. Scale bars - 10 μ m.

Supplementary Tables.

Supplementary Table 1. Staining different cell lines with SiR-actin and SiR-tubulin probes.

No.	Cell line name	Organism	Ref.	Provider	SiR-tubulin		SiR-actin	
					No verapamil	10 μ M verapamil	No verapamil	10 μ M verapamil
1	U2OS	Homo sapiens	4	ATCC	-/+	+	-/+	+
2	HeLa	Homo sapiens	5	Prof. Pierre Gönczy	+	N.D.	+	N.D.
3	Cos-7	Cercopithecus aethiops	6	DSMZ	-	-/+	-	-/+
4	Vero	Cercopithecus aethiops	7	ECACC	-	-	-	-
5	IA32	Mus musculus	8	Prof. James E. Bear	+	N.D.	+	N.D.
6	C2C12	Mus musculus	9	Prof. Urs Ruegg	-	+	-	+
7	NRK	Rattus norvegicus	10	Prof. Reiner Jahn	-/+	+	+	+
8	BHK	Mesocricetus auratus	11	Prof. Daniel Abankwa	+	+	+	+
9	Primary dermal fibroblasts	Homo sapiens	12	Lonza	+	+	+	+
10	Primary hippocampal neurons	Rattus norvegicus	13	Self-prepared	+	N.D.	+	N.D.

Specific signal estimated from wide field or confocal fluorescence microscopy images: “-” – no specific staining detected, “-/+” – not uniform staining of the cell population, “+” – specific uniform staining of the cell population. N.D. – not determined. Name in the provider field indicates that cell line was gift from another laboratory (see acknowledgements). “ATCC” stands for American Type Culture Collection, “ECACC” - European Collection of Animal Cell Cultures, DSMZ - Deutsche Sammlung von Mikroorganismen und Zellkulturen GmbH. Note: All the cell lines are mycoplasma negative (periodically checked). Primary hippocampal neurons were not checked for mycoplasma infection.

Supplementary Table 2. Properties of the synthesized probes.

Probe name	Specific signal in the cells*				In vitro activity	
	Living	MeOH fixed	PFA fixed	EGS fixed	Actin depolymerization assay**	Tubulin polymerization assay***
1	-	-	-	-	N.D.	No exp. growth phase
2	-	-	-	-	N.D.	0.37
3	+	-	-/+	+	N.D.	0.62
4, SiR-tubulin	+	-	-/+	+	N.D.	0.59
5	-	-	-	-	N.D.	No exp. growth phase
6	-	-	-/+	-/+	N.D.	0.20
7	+	-	+	N.D.	0.77	N.D.
8, SiR-actin	+	-	+	N.D.	0.93	N.D.
9	-	-	+	N.D.	0.62	N.D.

* - specific signal estimated from wide field fluorescence microscopy images: “-” – no specific staining detected, “-/+” – specific signal observed only in centrosomal region, “+” – specific staining of microtubules and centrosome detected. ** - number indicates relative amount of stabilized actin at steady state equilibrium phase relative to jasplakinolide (equal to 1), *** - number indicates tubulin polymerization rate relative to taxol (equal to 1). N.D. – not determined.

Supplementary Table 3. Physicochemical properties of the synthesized probes.

Probe name	LogD (pH 7.5)	QY		Excitation maximum (nm)*	Emission maximum (nm)*
		TBS	TBS + 0.2% SDS		
1	3.5	0.30	0.29	655	674
2	2.6	0.34	0.30	652	674
3	3.6	0.26	0.29	652	674
4, SiR-tubulin	4.4	0.13	0.30	652	672
5	6.0	0.08	0.32	652	672
6	4.4	N.D.	0.27	652	674
7	6.0	0.05	0.27	652	674
8, SiR-actin	6.1	N.D.	0.26	652	674
9	-3.1	0.15	0.28	652	674

Note: Fluorescence increase upon SDS addition is much bigger compared to QY changes due to the additional decrease in absorbance by spirolactonization of SiR. Relative quantum yields (QY) values obtained in TBS buffer (pH 7.4) containing 1 mg/ml BSA. SiR-carboxyl solution in PBS was used as reference with QY = 0.4. N.D. – not determined due to very low absorbance and fluorescence in the absence of SDS.

Supplementary notes

Supplementary Note 1. Design and properties of the SiR-tubulin probe. The simple direct conjugation of SiR to docetaxel yielded molecule **1** which did not stain microtubules in living cells and displayed low activity in the tubulin polymerization assay (**Supplementary Note 2** and **Supplementary Fig. 1a, 4 and 7b**). We hypothesized that the proximity of the fluorophore to docetaxel might interfere with binding to tubulin. Thus, we inserted hydrophobic linkers of different lengths ranging from three to twelve atoms as well as an analog containing a phenyl ring at the 3'-N-position followed by a six-carbon linker (**Supplementary Note 2** and **Supplementary Fig. 1a**). Wide field microscopy imaging revealed that probes **3** and **4** (SiR-tubulin) bearing linker lengths equal to six and eight carbon atoms are the only ones which showed specific tubulin staining and displayed increased activity in a tubulin polymerization assay (**Fig. 1c - d, Supplementary Fig. 1a, 4 and 7a,b**). Remarkably, the SiR-tubulin probe **4** showed a significantly higher fluorescence change upon binding to the target compared to probe **3** (**Fig. 1c** and **Supplementary Fig. 2c**). No staining of living cells and lower tubulin polymerization enhancement was observed using probes **5** and **6** bearing longer linkers (**Supplementary Fig. 1a, 4 and 7b**). Such results could be explained by reduced binding of docetaxel analogs to tubulin and/or poor cell membrane permeability. To investigate this further we have stained methanol, paraformaldehyde (PFA) and ethyleneglycol-bis-succinimidyl-succinate (EGS) fixed cells (**Supplementary Table 2**). Only EGS fixed cells have shown specific staining by probes **3** and **4**, which indicates that the absence of signal of the other probes is due to their insufficient binding affinity to microtubules. Other fixation methods (methanol and paraformaldehyde) seem to destroy the taxane binding site of microtubules (**Supplementary Table 2**). Similar observations were previously reported in literature for the fluorescent taxol (paclitaxel) derivative Flutax¹⁴.

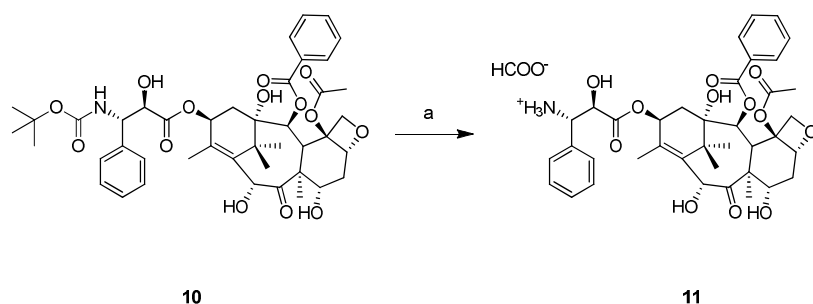
The reported conjugate of desbromo-desmethyl-jasplakinolide and tetramethylrhodamine, which is structurally similar to the SiR fluorophore, did not selectively stain actin in living cells¹⁵. However, the direct conjugation of SiR to the desbromo-desmethyl-jasplakinolide derivative yielded probe **7** (**Supplementary Note 2** and **Supplementary Fig. 1a**) which displayed a more than 55-fold increase in fluorescence upon binding to F-actin and stained actin in living cells (**Supplementary Fig. 2d and 5**). We have synthesized analogue **8** (SiR-actin) bearing a six-carbon

linker between the fluorophore and the targeting molecule resulting in a molecule, structurally related to the reported BODIPY® FL derivative (**Supplementary Note 2** and **Supplementary Fig. 1a**). Probe **8** displayed more than 100-fold increase in fluorescence upon F-actin binding and stained it inside living cells (**Supplementary Fig. 2b, 2d and 5**).

A conjugate of SiR and phalloidin (compound **9**) does not show significant fluorogenicity (**Supplementary Fig. 1b**). We assume this is due to the fact that the conjugate is not hydrophobic enough to shift the spirolactone-zwitterion equilibrium towards the spirolactone. This hypothesis is supported by the calculated Log D¹⁶, which are 6.1 and -3.1 for derivatives **8** and **9**, respectively (**Supplementary Table 3**). Furthermore, applying probe **9** to living cells did not result in any F-actin labeling (**Supplementary Fig. 5**). To confirm actin binding of the synthesized probes we have used them to stain fixed human primary dermal fibroblasts. We found that all SiR-based actin probes were able to stain actin in formaldehyde fixed cells which indicates that the phalloidin probe is binding actin but is not cell permeable (**Supplementary Fig. 14 and Supplementary Table 2**).

Supplementary Note 2. Chemical synthesis of tubulin and actin probes. All chemical reagents and anhydrous solvents for synthesis were purchased from commercial suppliers (Sigma-Aldrich, Fluka, Acros) and were used without further purification or distillation. The composition of mixed solvents is given by the volume ratio (v/v). ¹H and ¹³C nuclear magnetic resonance (NMR) spectra were recorded on a Bruker DPX 400 (400 MHz for ¹H, 100 MHz for ¹³C, respectively) or Bruker DRX-600 (600 MHz for ¹H, 151 MHz for ¹³C, respectively), with chemical shifts (δ) reported in ppm relative to the solvent residual signals of CDCl₃ (7.26 ppm for ¹H, 77.16 ppm for ¹³C), CD₃OD (3.31 ppm for ¹H, 49.00 ppm for ¹³C), DMSO-*d*₆ (2.50 ppm for ¹H, 39.52 ppm for ¹³C). Coupling constants are reported in Hz. High resolution mass spectra (HRMS) were measured on a Micromass Q-TOF Ultima spectrometer with electrospray ionization (ESI). LC-MS was performed on a Shimadzu MS2020 connected to a Nexerra UHPLC system equipped with a Waters ACQUITY UPLC BEH C18 1.7 μm 2.1x50 mm column. Buffer A: 0.05% HCOOH in H₂O Buffer B: 0.05% HCOOH in acetonitrile. Analytical gradient was from 5% to 95% B within 5.5 min with 0.5 ml/min flow. Preparative RP-HPLC was performed on a Dionex system equipped with an UVD 170U UV-Vis detector for product visualization on a Waters

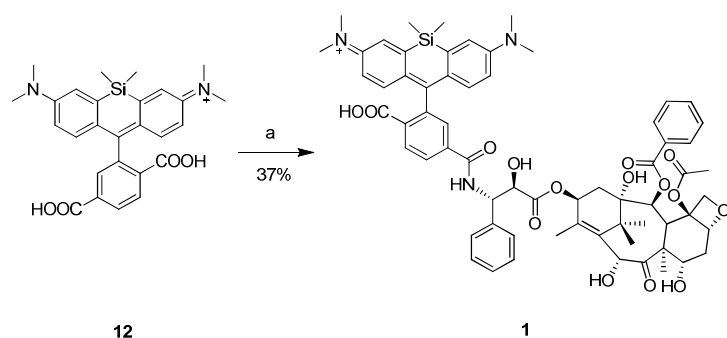
SunFire™ Prep C18 OBD™ 5 μm 10×150 mm Column. Buffer A: 0.1% TFA in H₂O
 Buffer B: acetonitrile. Typical gradient was from 0% to 100% B within 30 min with 4 ml/min flow. After lyophilization of HPLC purified compounds, the solid residue was generally dissolved in dry DMSO and the concentration of the SiR-derivatives was measured by UV-Vis spectroscopy in PBS containing 0.1% SDS, using the SiR molar extinction coefficient of 100'000 M⁻¹cm⁻¹ at 650 nm.



Synthetic route of docetaxel derivative **11**: (a) HCOOH, r.t.

3'-aminodocetaxel **11**

Docetaxel **10** (5 mg, 6.3 μmol, 1 eq) was dissolved in formic acid (0.2 ml) and incubated at r.t. for 30 min. The solvent was evaporated under reduced pressure and the residue was dried under high vacuum for 2h. The crude 3'-aminodocetaxel formate salt **11** was dissolved in anhydrous DMSO (125 μl) to give a 50 mM solution (assuming quantitative yield) and was used for the next step without further purification.

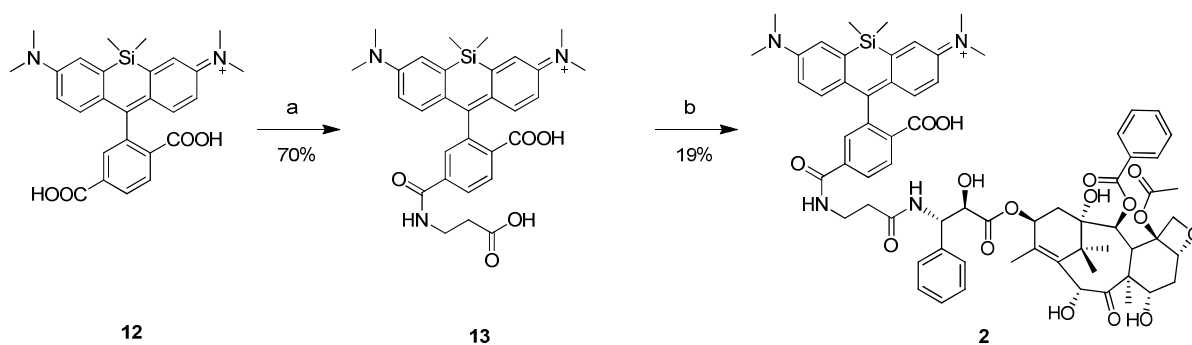


Synthetic route of tubulin probe **1**: (a) **11**, TSTU, DIEA, DMSO, r.t.

Tubulin probe **1**

SiR-carboxyl **12**¹⁷ (15 μl of a 20.0 mM solution in DMSO, 0.3 μmol, 1 eq.) was treated with DIEA (3 μl, 17.4 μmol, 58 eq.) and TSTU (4 μl of a 0.1 M solution in

DMSO, 0.4 μmol , 1.3 eq.). After 5 min, 3'-aminodocetaxel **11** (12 μl of a 50 mM solution in DMSO, 0.6 μmol , 2 eq.) was added and incubated for 1h at r.t. The product was purified by RP-HPLC, lyophilized and dissolved in dry DMSO. 100 μl of 1.1 mM solution of **1** were obtained (37% yield) as a light blue solution. LCMS: (LC: $t_{\text{R}} = 4.31$ min); HRMS (ESI) calcd for $\text{C}_{65}\text{H}_{72}\text{N}_3\text{O}_{15}\text{Si}^+$ $[\text{M}+\text{H}]^+$ 1162.4727; found 1162.4702.



Synthetic route of tubulin probe **2**: (a) i) β -Alanine ethyl ester hydrochloride, TSTU, DIEA, DMSO, r.t.; ii) aq. NaOH; (b) **11**, TSTU, DIEA, DMSO, r.t.

SiR-C3-COOH **13**

SiR-carboxyl **12**¹⁷ (7.2 mg, 15.2 μmol , 1 eq.) was dissolved in DMSO (0.5 ml). DIEA (20 μl , 116 μmol , 7.6 eq.) and TSTU (5.4 mg, 18.0 μmol , 1.2 eq.) were successively added. After 5 min, β -alanine ethyl ester hydrochloride (3.0 mg, 20 μmol , 1.3 eq.) was added. The mixture was incubated for 15 min at r.t. Then 2 M NaOH (200 μl) was added and the mixture was incubated for 15 min at r.t. AcOH was added until the pH was neutral and the reaction was purified by RP-HPLC, lyophilized and dissolved in DMSO. 400 μl of 26.8 mM solution of **13** (70% yield) were obtained as a dark blue solution.

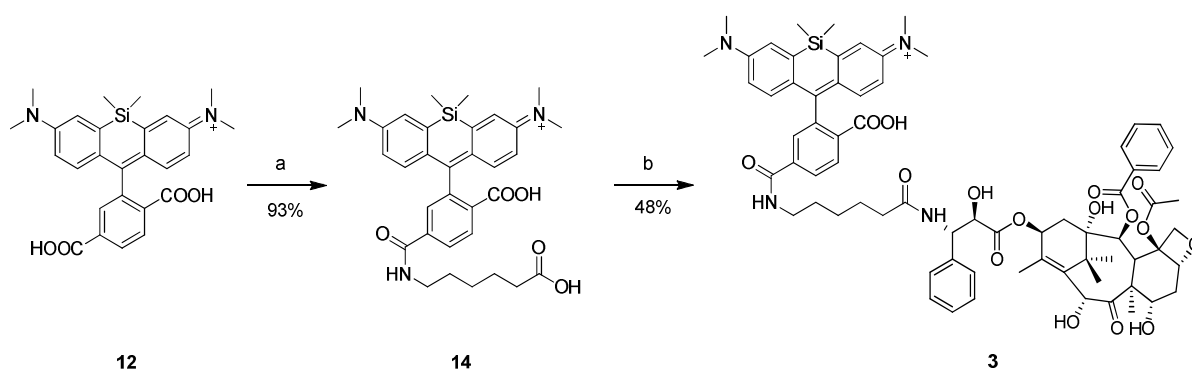
^1H NMR (400 MHz, DMSO) δ 8.81 (t, 1 H, $J = 5.2$ Hz), 8.08 (m, 2 H), 7.69 (s, 1 H), 7.14 (s, 2 H), 6.70 (m, 4 H), 3.43 (m, 2 H), 3.00 (s, 12 H), 2.49 (m, 2 H), 0.66 (s, 3 H), 0.49 (s, 3 H); LCMS: (LC: $t_{\text{R}} = 3.41$ min); HRMS (ESI) calcd for $\text{C}_{30}\text{H}_{34}\text{N}_3\text{O}_5\text{Si}^+$ $[\text{M}+\text{H}]^+$ 544.2262; found 544.2243.

Tubulin probe **2**

SiR-C3-COOH **13** (10 μl of 26.8 mM solution in DMSO, 0.27 μmol , 1 eq.) was treated with DIEA (2.5 μl , 14.5 μmol , 53 eq.) and TSTU (3 μl of a 0.1 M solution in DMSO,

0.32 μmol , 1.2 eq.). After 5 min, 3'-aminodocetaxel **11** (10 μl of a 50 mM solution in DMSO, 0.5 μmol , 1.9 eq.) was added. The mixture was incubated for 3 h at r.t. The product was purified by RP-HPLC, lyophilized and dissolved in DMSO. 50 μl of 1.0 mM solution of **2** were obtained (19% yield) as a light blue solution.

LCMS: (LC: t_{R} = 4.09 min); HRMS (ESI) calcd for $\text{C}_{68}\text{H}_{77}\text{N}_4\text{O}_{16}\text{Si}^+$ $[\text{M}+\text{H}]^+$ 1233.5098; found 1233.5106.



Synthetic route of tubulin probe **3**: (a) i) 6-aminohexanoic acid methyl ester, TSTU, DIEA, DMSO, r.t.; ii) aq. NaOH. (b) **11**, TSTU, DIEA, DMSO, r.t.

SiR-C6-COOH **14**

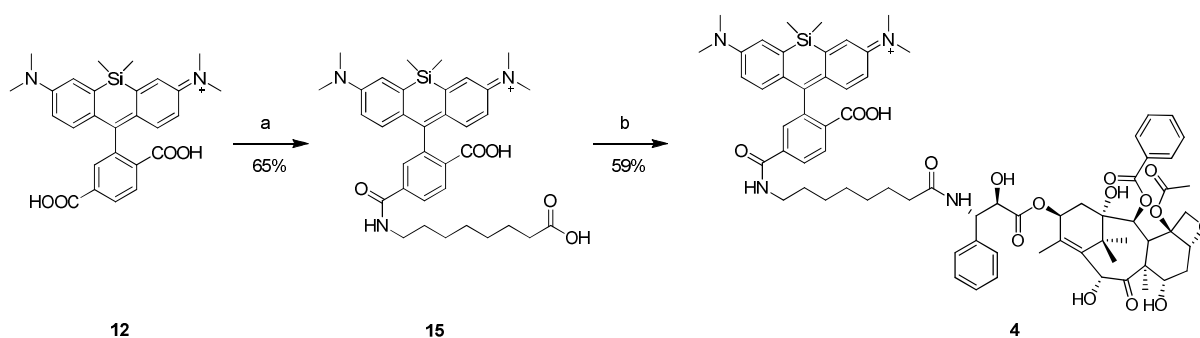
SiR-carboxyl **12**¹⁷ (31 mg, 66 μmol , 1 eq.) was dissolved in DMSO (1.0 ml). DIEA (30 μl , 174 μmol , 2.6 eq.) and TSTU (23 mg, 78 μmol , 1.2 eq.) were successively added. After 5 min, 6-aminohexanoic acid methyl ester (13.6 mg, 78 μmol , 1.2 eq.) was added. The mixture was incubated for 15 min at r.t. Then 2 M NaOH (200 μl) was added and the mixture was incubated for 15 min at r.t.. AcOH was added until the pH was neutral and the reaction was purified by RP-HPLC and lyophilized. 36 mg (93% yield) of **14** were obtained as a blue solid.

¹H NMR (400 MHz, MeOD) δ 8.17 (d, 1 H, J = 8.3 Hz), 7.99 (d, 1 H, J = 8.2 Hz), 7.59 (s, 1 H), 7.24 (s, 2 H), 6.86 (d, 2 H, J = 9.5 Hz), 6.65 (dd, 2 H, J = 2.5 Hz), 3.26 (t, 2 H, J = 6.6 Hz), 3.16 (s, 12 H), 2.18 (t, 2 H, J = 7.2 Hz), 1.52 (m, 4 H), 1.30 (m, 2 H), 0.54 (s, 3 H), 0.46 (s, 3 H); ¹³C NMR (101 MHz, MeOD) δ 176.13, 166.63, 153.30, 146.77, 142.66, 139.01, 137.77, 132.65, 130.51, 128.83, 128.26, 127.51, 120.35, 117.65, 114.77, 114.04, 39.79, 39.70, 33.42, 28.66, 26.20, -2.12, -3.05; LCMS: (LC: t_{R} = 3.68 min); HRMS (ESI) calcd for $\text{C}_{33}\text{H}_{40}\text{N}_3\text{O}_5\text{Si}^+$ $[\text{M}+\text{H}]^+$ 586.2732; found 586.2740.

Tubulin probe **3**

SiR-C6-COOH **14** (74 μ l of 13.5 mM solution in DMSO, 1.0 μ mol, 1 eq.) was treated with DIEA (5 μ l, 30 μ mol, 30 eq.) and TSTU (12 μ l of a 100 mM solution in DMSO, 1.2 μ mol, 1.2 eq.). After 5 min, 3'-aminodocetaxel **11** (22 μ l of a 50 mM solution in DMSO, 1.1 μ mol, 1.1 eq.) was added. The mixture was incubated for 5 h at r.t. The product was purified by RP-HPLC, lyophilized and dissolved in dry DMSO. 150 μ l of 3.2 mM solution of **3** were obtained (48% yield) as a light blue solution.

^1H NMR (400 MHz, DMSO) δ 8.70 (t, 1 H, $J = 5.4$ Hz), 8.36 (d, 1 H, $J = 9.0$ Hz), 8.03-8.10 (m, 2 H), 7.98 (d, 2 H, $J = 7.3$ Hz), 7.64-7.70 (m, 2 H), 7.59 (t, 2 H, $J = 7.7$ Hz), 7.27-7.38 (m, 4 H), 7.19 (t, 1 H, $J = 7.2$ Hz), 7.09 (br, s, 2 H), 6.68 (m, 4 H), 5.90 (t, 1 H, $J = 8.6$ Hz), 5.41 (d, 1 H, $J = 7.2$ Hz), 5.26 (dd, 1 H, $J = 6.0$ Hz), 5.09 (s, 1 H), 4.90 (d, 1 H, $J = 10.1$ Hz), 4.40 (d, 1 H, $J = 5.9$ Hz), 3.98-4.09 (m, 3 H), 3.68 (d, 1 H, $J = 7.1$ Hz), 3.17 (m, 2 H), 2.97 (s, 12 H), 2.20-2.32 (m, 4 H), 2.15 (t, 2 H, $J = 7.3$ Hz), 1.97 (dd, 1 H, $J = 9.4$ Hz), 1.59-1.86 (m, 5 H), 1.41-1.56 (m, 7 H), 1.24 (m, 2 H), 1.02 (s, 3 H), 0.98 (s, 3 H), 0.65 (s, 3 H), 0.53 (s, 3 H); ^{13}C NMR (151 MHz, DMSO) δ 209.82, 173.15, 172.32, 170.19, 165.73, 165.04, 140.11, 137.27, 136.39, 133.79, 130.53, 130.07, 129.16, 128.64, 128.59, 127.62, 114.51, 84.22, 80.81, 77.41, 75.95, 75.30, 74.26, 74.06, 71.30, 70.49, 57.48, 55.49, 46.46, 43.43, 40.55, 36.97, 35.83, 35.53, 29.20, 27.01, 26.63, 25.63, 22.90, 21.33, 14.16, 10.31; LCMS: (LC: $t_{\text{R}} = 4.23$ min); HRMS (ESI) calcd for $\text{C}_{71}\text{H}_{83}\text{N}_4\text{O}_{16}\text{Si}^+ [\text{M}+\text{H}]^+$ 1275.5568; found 1275.5526



Synthetic route of tubulin probe **4**: (a) 8-aminooctanoic acid TSTU, DIEA, DMSO, r.t.. (b) **11**, HBTU, DIEA, DMSO, r.t.

SiR-C8-COOH **15**

SiR-carboxyl **12**¹⁷ (4.0 mg, 8.5 μ mol, 1 eq.) was dissolved in DMSO (0.25 ml). DIEA (10 μ l, 58 μ mol, 6.8 eq.) and TSTU (3 mg, 10 μ mol, 1.2 eq.) were successively

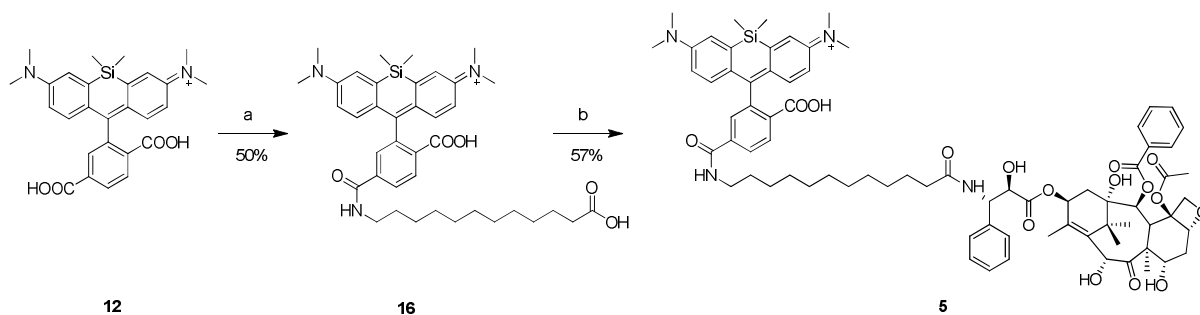
added. After 5 min, 8-aminooctanoic acid (3.2 mg, 20 μ mol, 2.3 eq.) was added. The reaction was sonicated 15 min at r.t. Then H₂O was added (50 μ l) and the mixture was incubated for 15 min at r.t. AcOH was added until the pH was neutral and the reaction was purified by RP-HPLC and lyophilized. 4.4 mg (84% yield) of **15** were obtained as a blue solid.

¹H NMR (400 MHz, DMSO) δ 8.79 (br, s, 1 H), 8.15 (br, s, 2 H), 7.75 (br, s, 1 H), 7.20 (br, s, 2 H), 6.78 (br, s, 4 H), 3.29 (m, 2H), 3.07 (s, 12 H), 2.25 (t, 2 H, J = 7.2 Hz), 1.54 (br, s, 4 H), 1.33 (br, s, 6 H), 0.73 (s, 3 H), 0.61 (s, 3 H); LCMS: (LC: t_R = 4.00 min); HRMS (ESI) calcd for C₃₅H₄₄N₃O₅Si⁺ [M+H]⁺ 614.3045; found 614.3055.

Tubulin probe **4** (SiR-tubulin)

SiR-C8-COOH **15** (300 μ l of a 18.2 mM solution in DMSO, 5.5 μ mol, 1 eq.) was treated with DIEA (50 μ l, 290 μ mol, 52 eq.) and HBTU (2.5 mg, 6.6 μ mol, 1.2 eq.). After 5 min, 3'-aminodocetaxel **11** (5.8 mg, 8.2 μ mol, 1.5 eq.) was added. The mixture was incubated overnight at r.t. The product was purified by RP-HPLC and lyophilized. 4.2 mg of **4** were obtained (59% yield) as a blue solid.

¹H NMR (600 MHz, DMSO) δ 8.72 (t, 1 H, J = 5.2 Hz), 8.37 (d, 1 H, J = 9.0 Hz), 8.10 (s, 2 H), 7.99 (d, 2 H, J = 7.9 Hz), 7.68 (m, 2 H), 7.60 (t, 2 H, J = 7.4 Hz), 7.29-7.38 (m, 4 H), 7.19 (m, 1 H), 6.76 (s, 4 H), 5.91 (t, 1 H, J = 8.9 Hz), 5.42 (d, 1 H, J = 7.2 Hz), 5.28 (dd, 1 H, J = 6.0 Hz), 5.10 (s, 1 H), 4.91 (d, 1 H, J = 9.9 Hz), 4.41 (d, 3 H, J = 5.8 Hz), 4.04 (m, 3 H), 3.69 (d, 1 H, J = 7.1 Hz), 3.21 (m, 2 H), 3.10 (m, 3 H), 2.21-2.30 (m, 3 H), 2.15 (m, 2 H), 1.98 (m, 1 H), 1.84 (m, 2 H), 1.67 (m, 1 H), 1.53 (s, 3 H), 1.46 (d, 4 H, J = 4.7 Hz), 1.16-1.28 (m, 6 H), 1.03 (s, 3 H), 0.99 (s, 3 H), 0.66 (s, 3 H), 0.54 (s, 3 H); ¹³C NMR (151 MHz, DMSO) δ 209.84, 173.14, 172.38, 170.20, 165.74, 164.95, 158.93, 140.13, 137.26, 136.40, 133.80, 130.52, 130.08, 129.17, 128.62, 128.54, 127.62, 115.09, 84.21, 80.80, 77.41, 75.94, 75.30, 74.26, 74.05, 71.30, 70.52, 57.47, 55.44, 46.46, 46.40, 46.37, 45.43, 43.42, 40.89, 40.52, 36.96, 35.86, 35.53, 29.42, 29.06, 29.02, 26.99, 26.93, 26.43, 26.37, 25.86, 24.11, 22.89, 21.32, 14.17, 10.31. LCMS: (LC: t_R = 4.44 min); HRMS (ESI) calcd for C₇₃H₈₇N₄O₁₆Si⁺ [M+H]⁺ 1303.5881; found 1303.5862.



Synthetic route of tubulin probe **5**: (a) **12**-aminododecanoic acid, TSTU, DIEA, DMSO, r.t.; (b) **11**, TSTU, DIEA, DMSO, r.t.

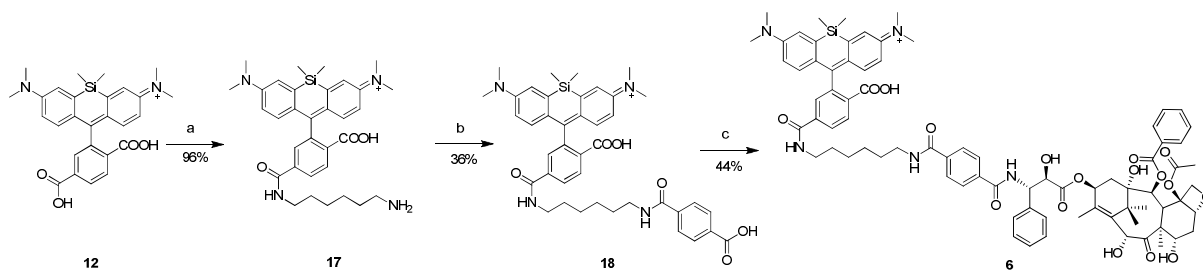
SiR-C12-COOH **16**

SiR-carboxyl **12**¹⁷ (30 μ l of a 20.0 mM solution in DMSO, 0.6 μ mol, 1 eq.) was treated with DIEA (2 μ l, 12 μ mol, 20 eq.) and TSTU (7 μ l of 100 mM DMSO solution, 0.7 μ mol, 1.2 eq.). After 5 min, 12-aminododecanoic acid (2.0 mg, 9.3 μ mol, 15 eq.) was introduced. The mixture was sonicated for 15 min and incubated for 4h at r.t with shaking. The mixture was purified by RP-HPLC, corresponding product fractions were combined, lyophilized and dissolved in dry DMSO. 50 μ l of 6.0 mM solution of **16** (50% yield) were obtained as a blue solution.

LCMS: (LC: t_R = 4.79 min); HRMS (ESI) calcd for $C_{39}H_{52}N_3O_5Si^+$ $[M+H]^+$ 670.3671; found 670.3663.

Tubulin probe **5**

SiR-C12-COOH **16** (50 μ l of a 6.0 mM solution in DMSO, 0.3 μ mol, 1 eq.) was treated with DIEA (2.5 μ l, 14.5 μ mol, 48 eq.) and TSTU (4 μ l of a 0.1 M solution in DMSO, 0.4 μ mol, 1.3 eq.). After 5 min, 3'-aminodocetaxel **11** (30 μ l of a 30 mM solution in DMSO, 0.9 μ mol, 3 eq.) was added. The mixture was incubated for 3 h at r.t. The product was purified by RP-HPLC, lyophilized and dissolved in dry DMSO. 100 μ l of a 1.7 mM solution of **5** were obtained (57% yield) as a light blue solution. LCMS: (LC: t_R = 5.01 min); HRMS (ESI) calcd for calcd for $C_{77}H_{95}N_4O_{16}Si^+$ $[M+H]^+$ 1359.6512; found 1359.6552.



Synthetic route of tubulin probe **6**: (a) i) *N*-Boc-1,6-diaminohexane, TSTU, DIEA, DMSO, r.t. ii) TFA; (b) i) terephthalic acid monomethyl ester, TSTU, DIEA, DMSO, r.t.; ii) aq. NaOH; (c) **11**, HBTU, DIEA, DMSO, r.t.

SiR-C6-NH₂ **17**

SiR-COOH **12** (10.4 mg, 22 μ mol, 1 eq.) was dissolved in DMSO/MeCN 1:2 (0.3 ml). DIEA (10 μ l, 58 μ mol, 2.6 eq.) and TSTU (7.9 mg, 26 μ mol, 1.2 eq.) were added. After 5 min, *N*-Boc-1,6-diaminohexane (7.1 mg, 33 μ mol, 1.5 eq.) was added. The mixture was incubated for 30 min at r.t.. The mixture was diluted with 5 ml H₂O and extracted with CH₂Cl₂ (2 x 5ml). The combined extracts were concentrated and the residue was dissolved in TFA (0.3 ml). After 10 min, the solvent was evaporated, the residue was taken up in MeCN/H₂O 1:1 (1 ml), purified by RP-HPLC and lyophilized. 12.1 mg of **17** were obtained (96% yield) as a dark blue solid.

¹H NMR (400 MHz, DMSO) δ 8.75 (t, 1 H, J = 5.5 Hz), 8.07 (m, 2 H), 7.66 (s, 4 H), 7.09 (s, 2 H), 6.69 (m, 4 H), 3.23 (q, 2 H, J = 6.6 Hz), 2.97 (s, 12 H), 2.77 (m, 2 H), 1.50 (m, 4 H), 1.29 (dd, 4 H, J = 3.4 Hz), 0.65 (s, 3 H), 0.54 (s, 3 H); (LC: t_R = 3.11 min); HRMS (ESI) calcd for C₃₃H₄₄N₄O₃Si⁺ [M+2H]²⁺ 286.1586; found 286.1589.

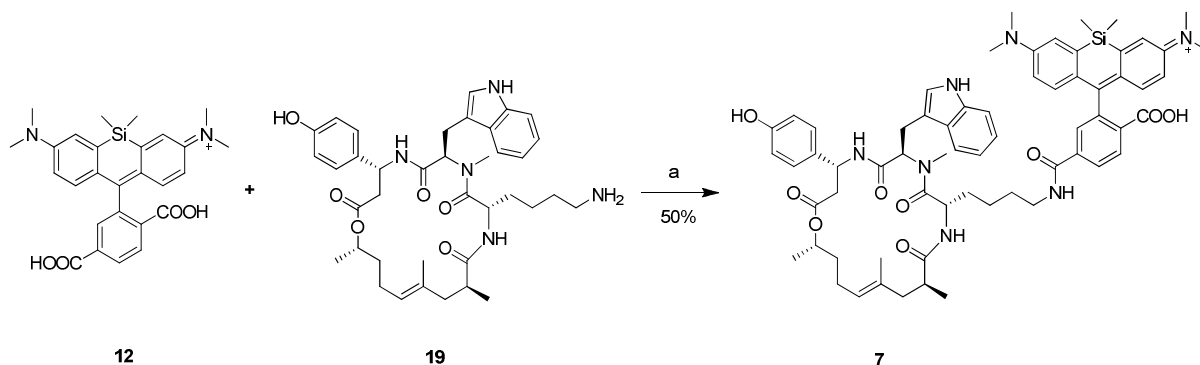
SiR-C6-Tpht-COOH **18**

Terephthalic acid monomethyl ester (30 μ l of a 0.1 M solution in DMSO, 3.0 μ mol, 2 eq.) was treated with DIEA (10 μ l, 58 μ mol, 19 eq.) and TSTU (30 μ l of a 0.1 M solution in DMSO, 3 μ mol, 2 eq.). After 5 min, SiR-C6-NH₂ **17** (30 μ l of a 50 mM solution in DMSO, 1.5 μ mol, 1 eq.) was added. After 15 min, 1M NaOH (0.1 ml) was added and the mixture was incubated for 15 min at r.t.. AcOH was then added until the pH was neutral and the mixture was purified by RP-HPLC. Product fractions were combined, lyophilized and dissolved in dry DMSO. 200 μ l of 2.7 mM solution of **18** (36% yield) were obtained as a blue solution.

LCMS: (LC: t_R = 3.80 min); HRMS (ESI) calcd for C₄₁H₄₇N₄O₆Si⁺ [M+H]⁺ 719.3259; found 719.3236.

Tubulin probe **6**

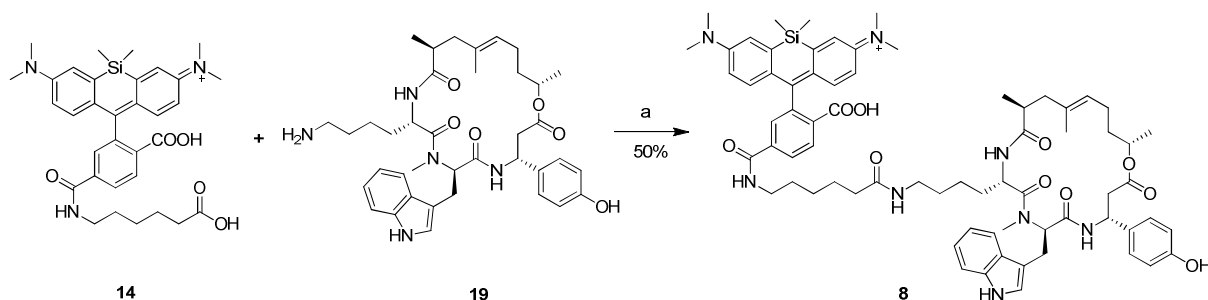
SiR-C6-Tpht-COOH **18** (50 μ l of a 2.7 mM solution in DMSO, 0.13 μ mol, 1 eq.) was treated with DIEA (5 μ l, 29 μ mol, 223 eq.) and HBTU (1 mg, 2.7 μ mol, 200 eq.). After 5 min, 3'-aminodocetaxel **11** (50 μ l of a 17 mM solution in DMSO, 0.85 μ mol, 6.5 eq.) was added. The mixture was incubated for 1 h at r.t. The product was purified by RP-HPLC. Product fractions were combined, lyophilized and dissolved in dry DMSO. 50 μ l of 1.2 mM solution of **6** were obtained (44% yield) as a light blue solution. LCMS: (LC: t_R = 4.31 min); HRMS (ESI) calcd for $C_{79}H_{90}N_5O_{17}Si^+$ $[M+H]^+$ 1408.6101; found 1408.6117.



Synthetic route of actin probe **7**: (a) TSTU, DIEA, DMSO, r.t.

Actin probe **7**

SiR-COOH **12** (75 μ l of a 10.0 mM solution in DMSO, 0.75 μ mol, 1 eq.) was treated with DIEA (2.5 μ l, 14.5 μ mol, 19 eq.) and TSTU (10 μ l of a 100 mM solution in DMSO, 1.0 μ mol, 1.3 eq.). After 5 min, lysine modified depsipeptide **19**¹⁵ (30 μ l of a 25 mM DMSO solution, 0.75 μ mol, 1 eq.) was added. The mixture was incubated for 1 h at r.t. The product was retrieved by RP-HPLC, lyophilized and dissolved in dry DMSO. 250 μ l of 1.5 mM solution of **7** were obtained (50% yield) as a blue solution. LCMS: (LC: t_R = 4.59 min); HRMS (ESI) calcd for $C_{65}H_{78}N_7O_9Si^+$ $[M+H]^+$ 1128.5625; found 1128.5585.

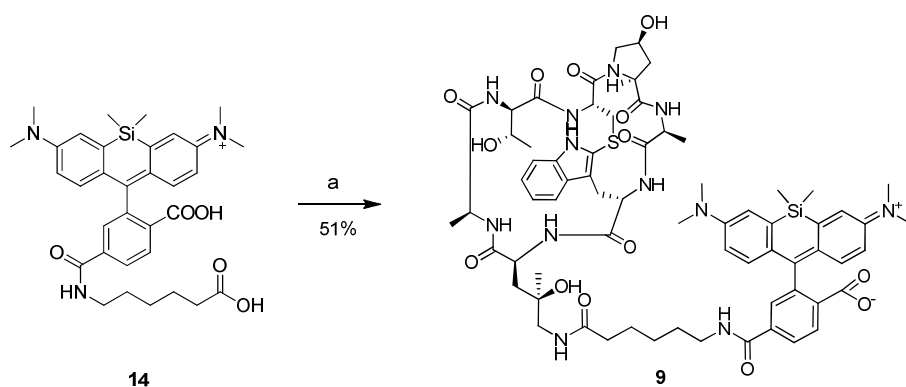


Synthetic route of actin probe **8**: (a) TSTU, DIEA, DMSO, r.t.

Actin probe **8** (SiR-actin)

SiR-C6-COOH **14** (60 μ l of 7.0 mM solution in DMSO, 0.42 μ mol, 1 eq.) was treated with DIEA (2.5 μ l, 14.5 μ mol, 34 eq.) and TSTU (10 μ l of a 50 mM solution in DMSO, 0.5 μ mol, 1.2 eq.). After 5 min, lysine modified depsipeptide **19**¹⁵ (17 μ l of a 25 mM DMSO solution, 0.42 μ mol, 1 eq.) was added. The mixture was incubated for 1 h at r.t. The product was retrieved by RP-HPLC, lyophilized and dissolved in dry DMSO. 150 μ l of 1.4 mM solution of **8** were obtained (50% yield) as a light blue solution.

¹H NMR (600 MHz, DMSO) δ 10.82 (s, 1 H), 9.32 (br, s, 1 H), 8.74 (t, 1 H, J = 5.5 Hz), 8.67 (d, 1 H, J = 8.8 Hz), 8.01-8.12 (m, 2 H), 7.62-7.73 (m, 4 H), 7.28 (d, 1 H, J = 8.0 Hz), 7.13 (d, 2 H, J = 8.6 Hz), 6.91-7.11 (m, 6 H), 6.63-6.73 (m, 6 H), 5.52 (dd, 1 H, J = 4.9 Hz), 5.19 (m, 1 H), 4.92 (t, 1 H, J = 6.5 Hz), 4.67 (m, 1 H), 4.55 (m, 1 H), 3.21 (m, 5 H), 3.01-3.07 (m, 5 H), 2.68 (m, 1 H), 2.44 (s, 2 H), 2.09 (s, 12 H), 2.02 (t, 2 H, J = 7.5 Hz), 1.84 (m, 2 H), 1.48 (s, 8 H), 1.39 (m, 2 H), 1.25 (m, 2 H), 1.16 (m, 4 H), 1.07 (dd, 2 H, J = 7.1 Hz), 0.92 (d, 3 H, J = 6.8 Hz), 0.81 (m, 3 H), 0.65 (s, 3 H), 0.53 (s, 3 H); LCMS: (LC: t_R = 4.38 min); HRMS (ESI) calcd for C₇₁H₈₉N₈O₁₀Si⁺ [M+H]⁺ 1241.6465; found 1241.6426.



Synthetic route of actin probe **9**: (a) 7-(5-Amino-4-hydroxy-L-leucine)phalloidin, TSTU, DIEA, DMSO, r.t.

Actin probe **9**

SiR-C6-COOH **14** (75 μ l of a 20.0 mM solution in DMSO, 1.5 μ mol, 1.2 eq.) was treated with DIEA (5 μ l, 29 μ mol, 24 eq.) and TSTU (17 μ l of a 100 mM solution in DMSO, 1.7 μ mol, 1.4 eq.). After 5 min, 7-(5-amino-4-hydroxy-L-leucine)phalloidin (1 mg dissolved in 50 μ l DMSO, 1.25 μ mol, 1.0 eq.) was added. The mixture was

incubated for 1 h at r.t. The product was purified by RP-HPLC, lyophilized and dissolved in dry DMSO. 200 μ l of a 3.2 mM solution of **9** were obtained (51% yield) as a blue solution. LCMS: (LC: t_R = 3.43 min); HRMS (ESI) calcd for $C_{77}H_{95}N_4O_{16}Si^+$ $[M+H]^+$ 1359.6507; found 1359.6547.

Supplementary Note 3. Toxicity of the SiR-tubulin and SiR-actin probes. We have not observed off-target staining which indicates that our tubulin probes are not binding to other taxol targets such as Bcl-2¹⁸. Despite the perturbation on mitotic progression in long-term imaging (**Supplementary Fig. 9**), 2 μ M SiR-tubulin had no detectable effect on the morphology of the interphase microtubule cytoskeleton.

Jasplakinolide induces polymerization of monomeric actin into amorphous aggregates and interferes with cell proliferation¹⁹. We have observed that the SiR-actin probe, similarly to previously reported BODIPY® FL derivative, did not show significant toxicity (tested up to 3.2 μ M). In contrast, jasplakinolide, was highly toxic already at low concentrations (**Supplementary Fig. 8, 9**)¹⁵. This is consistent with *in vitro* actin polymerization data, which indicate that the SiR-actin probe is not inducing actin polymerization, but rather stabilizes already polymerized actin filaments (**Supplementary Fig. 7c-f**). This stabilization, however, does not seem to interfere with dynamic actin networks in live cells, as cytokinetic cleavage furrow ingression in HeLa cells was unaffected by SiR-actin (**Supplementary Fig. 9**). The reduced toxicity of SiR-based probes might be a consequence of self-aggregation resulting in low concentration of monomers which are responsible for binding to the target proteins. Alternatively, the presence of the dye might favorably affect cytoskeletal superstructure or lead to a reduced incorporation frequency into the fiber.

Supplementary references

1. Rappaz, B. et al. *Cytometry A* **73**, 895-903 (2008).
2. Schindelin, J. et al. *Nat Methods* **9**, 676-682 (2012).
3. Riedl, J. et al. *Nat Methods* **5**, 605-607 (2008).
4. Niforou, K.M. et al. *Cancer Genomics Proteomics* **5**, 63-78 (2008).
5. Balestra, F.R., Strnad, P., Fluckiger, I. & Gonczy, P. *Dev Cell* **25**, 555-571 (2013).
6. Gluzman, Y. *Cell* **23**, 175-182 (1981).
7. Desmyter, J., Melnick, J.L. & Rawls, W.E. *J Virol* **2**, 955-961 (1968).
8. Cai, L., Makhov, A.M., Schafer, D.A. & Bear, J.E. *Cell* **134**, 828-842 (2008).
9. Yaffe, D. & Saxel, O. *Nature* **270**, 725-727 (1977).
10. de Larco, J.E. & Todaro, G.J. *J Cell Physiol* **94**, 335-342 (1978).
11. Stoker, M. & Macpherson, I. *Nature* **203**, 1355-1357 (1964).
12. Layman, D.L., Jelen, B.J. & Illingworth, D.R. *Proc Natl Acad Sci U S A* **77**, 1511-1515 (1980).
13. Godfrey, E.W., Nelson, P.G., Schrier, B.K., Breuer, A.C. & Ransom, B.R. *Brain Res* **90**, 1-21 (1975).
14. Evangelio, J.A. et al. *Cell Motil Cytoskeleton* **39**, 73-90 (1998).
15. Milroy, L.G. et al. *J Am Chem Soc* **134**, 8480-8486 (2012).
16. Kah, M. & Brown, C.D. *Chemosphere* **72**, 1401-1408 (2008).
17. Lukinavicius, G. et al. *Nat Chem* **5**, 132-139 (2013).
18. Ferlini, C. et al. *Cancer Res* **69**, 6906-6914 (2009).
19. Bubb, M.R., Spector, I., Beyer, B.B. & Fosen, K.M. *J Biol Chem* **275**, 5163-5170 (2000).